ACS APPLIED MATERIALS & INTERFACES

Research Article

www.acsami.org

Efficient Sorption of Cu^{2+} by Composite Chelating Sorbents Based on Potato Starch-*graft*-Polyamidoxime Embedded in Chitosan Beads

Ecaterina Stela Dragan,* Diana Felicia Apopei Loghin, and Ana Irina Cocarta

"Petru Poni" Institute of Macromolecular Chemistry, Grigore Ghica Voda Alley 41 A, Iasi 700487, Romania

ABSTRACT: Ionic composites based on cross-linked chitosan (CS) as matrix and poly(amidoxime) grafted on potato starch (AOX) as entrapped chelating resin were prepared as beads, for the first time in this work, by two strategies: (1) thorough mixing of previously prepared AOX in the CS solution followed by the bead formation and (2) thorough mixing of the potato starch-*g*-poly(acrylonitrile) (PS-*g*-PAN) copolymer in the initial CS solution, followed by bead formation, the amidoximation of the nitrile groups taking place inside the beads. Ionotropic gelation in tripolyphosphate was used to obtain the composite beads, and in situ covalent cross-linking by epichlorohydrin was carried out to stabilize the beads in the acidic pH range. Fourier transform infrared spectroscopy and the swelling ratio values in the acidic pH range confirmed the influence of the synthesis strategy on the structure of the CS/AOX composites. Scanning electron microscopy was employed to reveal the morphology of the novel composites, both before and after their loading with Cu^{2+}. The binding capacity of Cu^{2+} ions as a function of sorbent composition, synthesis strategy, pH, sorbent dose, contact time, initial concentration of Cu^{2+}, and temperature was examined in batch mode. The main difference between the composites prepared with the two strategies consisted of the higher sorption capacity and the much faster settlement of the equilibrium sorption for the composite prepared by the in situ amidoximation of PS-*g*-PAN. The Langmuir, Freundlich, Temkin, Dubinin−Radushkevich, and Sips isotherms were applied to fit the sorption equilibrium data. The maximum equilibrium sorption capacity, q_m, evaluated by the Langmuir model at 25 °C was 133.15 mg Cu^{2+}/g for the CS/AOX composite beads prepared with the first strategy and 238.14 mg Cu^{2+}/g for the CS/AOX composite beads prepared with the second strategy, at the same AOX content. The pseudo-second order kinetic model well fitted the sorption kinetics data, supporting chemisorption as the mechanism of interaction between the chelating composites and the Cu^{2+} ions. The CS/AOX composite sorbents could be reused up to five sorption/desorption cycles with no significant decrease in Cu^{2+} sorption capacity.

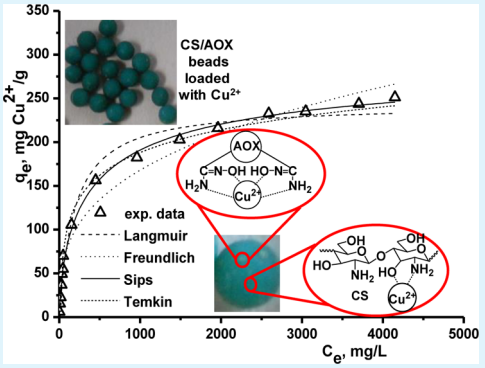

KEYWORDS: *chitosan, composite, potato starch, poly(amidoxime), copper*

1. INTRODUCTION

Pollution of water and soil by heavy metal ions is considered extremely hazardous to the environment because of their nonbiodegradability, high toxicity, and carcinogenic effect. Inadequately treated effluents transport heavy metals to water bodies, where they accumulate in aquatic organisms and are further transferred to the human body through the food chain. Among the conventional technologies used for the heavy metal removal, such as chemical treatment, evaporation, electrolysis, membrane separation, ion exchange, separation/enrichment by sorption, and biological processes, adsorption is considered superior to the other techniques in terms of low costs and operation. Other advantages of adsorption include the flexibility in the selection of the adequate sorbent, and the possibility of enriching the trace metal amounts.[1,2]

The use of sorbents derived from polysaccharides, as a more cost-effective alternative to the existing sorbents such as activated carbon and synthetic ion exchangers, has lately attracted considerable interest.[3−13] Chitosan (CS) is a linear cationic semisynthetic polysaccharide, composed of β-(1−4)-2-amino-2-deoxy-D-glucopyranose and β-(1−4)-2-acetamido-2-deoxy-D-glucopyranose units, obtained by deacetylation of its parent natural polymer chitin. Among biopolymers, CS has a special position due to its outstanding properties such as biocompatibility, antibacterial activity, high mechanical strength, film forming properties, which recommend it for numerous biomedical applications.[14] Moreover, the abundance of hydroxyl, acetamido and amino functional groups in CS generates hydrophilicity and excellent chelating properties for heavy metal ions.[3−10] On the other hand, sorbents containing amidoxime functional groups show a high tendency of chelation with transition and heavy metal ions, such as UO_2^{2+}, Cu^{2+}, Cd^{2+}, Fe^{3+}, As^{3+}, and Zn^{2+} in aqueous solutions.[15−24] It has been observed that sorbents containing both amidoxime groups and other hydrophilic groups, such as hydroxyl, carboxyl, and amide, have a much higher sorption capacity for metal ions. Therefore, some sorbents based on polysaccharides grafted with poly(amidoxime), generated by the reaction between

Received: May 15, 2014
Accepted: September 5, 2014
Published: September 5, 2014

   dx.doi.org/10.1021/am504480q | ACS Appl. Mater. Interfaces 2014, 6, 16577−16592

hydroxylamine and the nitrile groups in polysaccharide-*g*-poly(acrylonitrile), and their capacity to bind heavy metal ions have been reported.[25,26]

In trace amounts, copper is one of the essential nutrients for humans, its deficiency being associated with anemia, and bone abnormalities. However, large doses of Cu^{2+} can produce health problems, such as gastrointestinal illnesses, the Cu^{2+} overload having cytotoxic effects on human lung and liver cells.[27] Strict control of Cu^{2+} concentration in wastewaters is vital, and therefore various novel systems have been designed for this target,[28−32] many of them being based on renewable resources.[5−11,33−38] This prompted us to investigate the preparation of novel composite chelating sorbents composed of poly(amidoxime) grafted on potato starch (AOX) entrapped in CS beads, both AOX and CS having chelating functional groups very efficient in binding metal ions, and then to correlate their structure with the binding efficiency of Cu^{2+} in aqueous solution. Two strategies were adopted for the synthesis of such composite sorbents: (1) thorough mixing of the previously prepared AOX in the CS solution followed by the ionotropic gelation in sodium tripolyphosphate (TPP) and (2) thorough mixing of the potato starch-*g*-poly(acrylonitrile) (PS-*g*-PAN) copolymer in the initial CS solution, followed by bead formation, the amidoximation of the nitrile groups taking place inside the beads. As has already been shown,[39−41] the CS beads ionically cross-linked by TPP have some advantages compared to those formed in NaOH: (1) the time required to form beads decreases from 24 h in NaOH to 4−5 h in TPP, and (2) the beads are more rigid due to the ionic interaction between the multivalent ions $P_5O_{10}^{5-}$ in TPP and the NH_3^+ ions in CS in acidic pH.[42] To make the CS beads insoluble in acid medium, chemical cross-linking with various cross-linkers such as glutaraldehyde,[9,33,39,43] ethylene glycol diglycidylether,[39,43] and epichlorohydrin (ECH)[5,39,40,43] has been reported. Among these cross-linkers, ECH has numerous applications in the preparation of polyamide−ECH polymers used to increase the wet-strength of paper,[44] and as cross-linking agent in the production of Sephadex size-exclusion chromatographic resins from dextrans. In this work, ECH was used as chemical cross-linker because the covalent bonds, which are generated during the cross-liking process, are chemically stable on the whole range of pH. A high chemical stability is required for a sorbent during the consecutive sorption/desorption cycles, when both acids and bases are usually used. The chelating composites were characterized by Fourier transform infrared spectroscopy (FT-IR), equilibrium water uptake, optical microscopy and scanning electron microscopy (SEM). The sorption capacity of the newly synthesized composite beads for Cu^{2+}, as a function of the sorbent composition, sorbent dose, pH, contact time, initial concentration of metal ion, and temperature was investigated in the paper. To the best of our knowledge, this is the first study on the synthesis of CS beads containing encapsulated amidoximated PS and on their sorption capacity for Cu^{2+}. Also, in the present work we address questions on the binding mechanism of Cu^{2+} ions and on the behavior of the composite sorbents during the successive sorption−desorption cycles.

2. MATERIALS AND METHODS

2.1. Materials. Potato starch (PS) from Fluka, moisture content <10%, was used as received. Acrylonitrile (AN) was distilled at about 77 °C and kept at low temperature. ECH was distilled twice on KOH. $CuSO_4·5H_2O$, H_2SO_4, NaOH, methanol p.a., and hydroxylamine chlorohydrate ($NH_2OH·HCl$) (Fluka) were used as received. The CS of low molar mass, purchased from Sigma-Aldrich, was used as received. The average molar mass, determined by viscometry,[45] was 467 kDa. The degree of acetylation (DA) of CS was evaluated by infrared spectroscopy, using a Vertex 70 Bruker FTIR spectrometer.[6,46] An average value of DA = 15%, resulting from three measurements, was taken into account.

2.2. Preparation of AOX. AOX was prepared by the amidoximation reaction of the nitrile groups in the PS-*g*-PAN copolymer with NH_2OH, as reported for other polymers.[18,26,47] For this purpose, PS-*g*-PAN copolymer was first prepared by the redox initiation of AN grafting on PS by Ce^{4+} ions.[48,49] The reaction of PS-*g*-PAN with NH_2OH took place according to Scheme 1.[18,26] The synthesis of the AOX copolymer was

Scheme 1. Preparation of AOX from the PS-*g*-PAN Copolymer

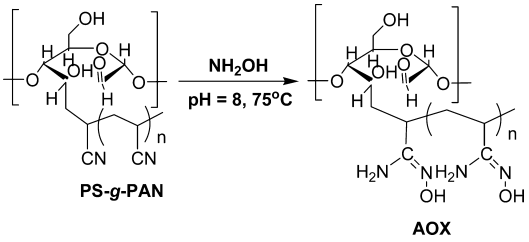

performed as follows. A solution of NH_2OH in methanol was first prepared by adding an equimolar amount of NaOH as aqueous solution, with a concentration of 12 g/L, to 11 g of $NH_2OH·HCl$ dissolved in 60 mL of methanol, and magnetically stirred for 2 h at 50 °C.

The final pH was adjusted to 7−8 with CH_3COOH, this pH range being recently reported as optimum for the amidoximation of cyanoethyl cellulose.[50] Typically, 1 g of PS-*g*-PAN was dispersed in a mixture of 15 mL *N*,*N*-dimethylformamide and 15 mL solution of NH_2OH in methanol with a concentration of ∼4.5%, the reaction being carried out at 75 °C for 20 h, the molar ratio NH_2OH/CN being around 2:1. The AOX copolymer, recovered by filtration as a white-yellow powder, was washed with methanol, and finally intensively washed with distilled water to neutral pH.

2.3. Preparation of CS/AOX Composite Beads. The synthesis conditions of the chelating composites are summarized in Table 1.

The overall code of the composites is CS_xAOX_y, wherein: CS stands for chitosan, AOX for amidoximated PS, x shows the mass percentage of CS in the total mixture of polymers, and y = 100-x shows the mass percentage of AOX. For example, $CS_{80}AOX_{20}$ means 80 wt % of CS and 20 wt % of AOX. The last figure in the code of samples $CS_{80}AOX_{20}$-A.1 and $CS_{80}AOX_{20}$-A.2 indicates: (1) composite synthesis by thorough mixing of the previously prepared AOX in the CS solution (1st strategy, Scheme 2A), and (2) composite synthesis by thorough mixing of the PS-*g*-PAN in the initial CS solution, followed by beads formation, the amidoximation of the nitrile groups occurring inside the beads (2nd strategy, Scheme 2B).

As shown in Scheme 2A, the preparation of CS_xAOX_y as beads according to the first strategy consisted of the following steps: (1) formation of beads by dropping the mixture formed from the AOX powder thorough dispersed in CS solution, and ECH calculated for a certain molar ratio ECH:NH_2, according to Table 1, into an aqueous solution of 0.05 M TPP, at 37 °C, and mild stirring for 4 h at this temperature, as previously

Table 1. Feed Composition, Cross-Linking Conditions, and Water Uptake of Chitosan/AOX Composites

			cross-linking Conditions			*W* (g/g)	
sample	ECH/CS molar ratio	AOX/CS, wt./wt.	TPP, 37 °C, h	0.1 M NaOH, 37 °C, h	0.1 M NaOH, 25 °C, h	pH = 2	pH = 5.5
$CS_{80}AOX_{20}$-A.1	1.7:1	0.25:1	4	2		4.7	1.7
$CS_{80}AOX_{20}$-A.2[a]	1.7:1	0.25:1	4	2		35	5.0
$CS_{80}AOX_{20}$-B	1.7:1	0.25:1	4	2	14	2.6	2.4
$CS_{80}AOX_{20}$-C	1.2:1	0.25:1	4	2			
$CS_{75}AOX_{25}$	1.7:1	0.34:1	4	2		6.5	3.8

[a]The sample was prepared by the in situ amidoximation of the nitrile groups contained in the preformed beads.

Scheme 2. Idealized Steps of the Two Synthesis Strategies Developed to Generate CS_xAOX_y Composite Beads: (A) Previously Prepared AOX (Peach Shaded Circle) Was Thorough Dispersed in the CS Solution before the Bead Formation and (B) PS-*g*-PAN as White Powder (Gray Shaded Circle) Was Thorough Dispersed in the CS Solution, the Amidoximation Being Performed in Situ after the Bead Formation

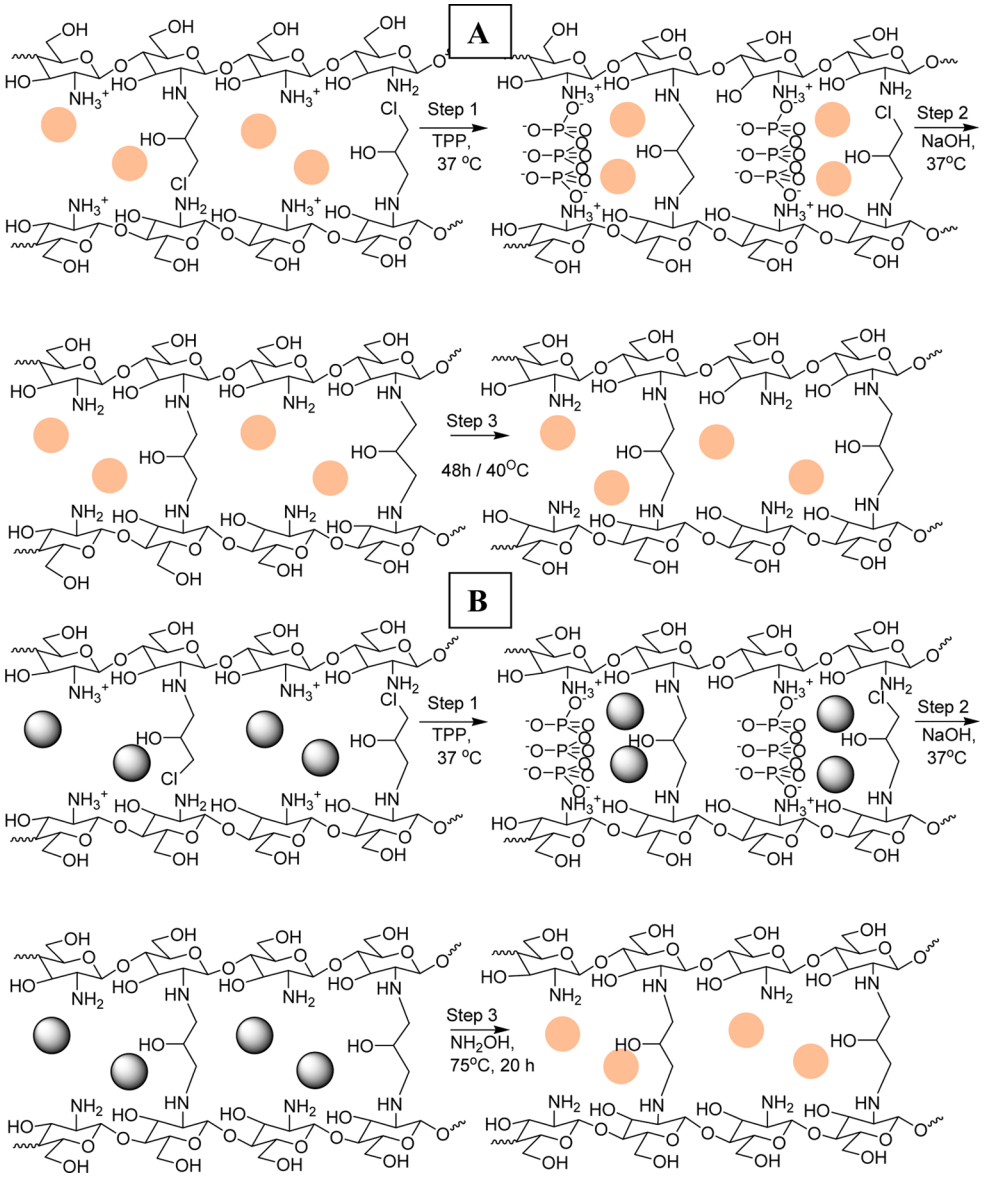

shown for other chitosan based composite beads;[6,34] (2) the ionically cross-linked beads were separated from the aqueous solution of TPP and transferred into a reactor containing 0.1 M NaOH, and agitated according to the thermal regime specified in Table 1; (3) thermal treatment for 48 h in vacuum, at 48 °C.

The synthesis of the composite $CS_{80}AOX_{20}$-A.1 is given as an example. In a typical synthesis procedure, 0.3 g of AOX powder were added step-by-step to 60 g of CS solution with a concentration of 2 wt % (in 1 vol % acetic acid solution), under vigorous magnetic stirring, and kept under stirring for 1 h at least. ECH (0.96 mL) was dropwise added, and kept under

stirring for 30 min, the final pH of the mixture being 4.0. To form beads, the mixture of CS, AOX and ECH in water was dropped by a syringe into 180 mL of 0.05 M TPP, under mild stirring, and kept for 4 h at 37 °C. Then, the beads were filtered off, and transferred into 120 mL of 0.1 M NaOH at 37 °C, for 2 h. The microspheres thus prepared were collected, rinsed with Milli pore water to neutral pH, dehydrated with methanol, filtered off and dried for 24 h at room temperature and for 48 h under vacuum at 40 °C.

For the preparation of composite $CS_{80}AOX_{20}$-A.2 (Table 1), 0.23 g of PS-*g*-PAN powder were thorough mixed with 60 g CS solution with a concentration of 2 wt % (in 1 vol % CH_3COOH), under vigorous magnetic stirring, and kept under stirring for 1 h at least. ECH (0.96 mL) was dropped under stirring, and stirring was maintained for 30 min. As shown in Scheme 2B, the formation of beads was performed similarly to the first strategy, by dropping the as prepared mixture into the 3-fold volume of an aqueous solution of 0.05 M TPP, under mild stirring, and keeping it for 4 h at 37 °C. Then, the beads were filtered off, and transferred into 120 mL of 0.1 M NaOH at 37 °C, for 2 h. The microspheres were collected, intensively rinsed with Milli pore water, and transferred into a three-neck reactor with 10 mL of DMF. For the in situ amidoximation, a solution of NH_2OH in ethanol/water (5/1, v/v) was first prepared as follows. 2.5 g of $NH_2OH.HCl$ were dissolved in 25 mL of ethanol/water (5/1, v/v), and then 1.4 g of NaOH were added under stirring, and the mixture was kept at 50 °C, for 2 h. After adjusting the pH to ~8, the NH_2OH solution was added into the reactor containing the CS/PS-*g*-PAN composite microspheres and then the temperature was maintained at 75 °C, for 20 h. The light-pink composite beads thus obtained were filtered off and intensively rinsed with Milli pore water to neutral pH, dehydrated with methanol, dried at room temperature, for 24 h and at 40 °C, for 48 h.

2.4. Composite Characterization. The structure of the CS_xAOX_y composites was investigated by FT-IR spectroscopy as a function of the synthesis conditions. The hydrated samples were first frozen in liquid nitrogen, then crushed into powder in a mortar and dried under vacuum in the presence of P_2O_5 for 1 day. FT-IR spectra were recorded with a Bruker Vertex FT-IR spectrometer, resolution 2 cm^{-1}, in the range of 4000−400 cm^{-1} by the KBr pellet technique, the amount of the sample being about 5−8 mg in each pellet.

Swelling behavior of the composite microspheres was studied by the conventional gravimetric procedure, immersing the completely dried samples in water at pH = 2 and pH = 5.5, at 25 °C, for 48 h. The swollen beads were weighed by an electronic balance, after wiping the excess surface liquid by filter paper, the water uptake, W (g/g), being calculated by eq 1:

$$W = \frac{W_{eq} - W_d}{W_d} \quad (1)$$

where W_d and W_{eq} are the weights (g) of the sample in dried state and swollen at equilibrium, respectively. The measurements were performed in three replicates and average data were used for calculation of W.

The optical microscope was used to show the size and shape of the wet and dry beads with various compositions. The surface and internal morphology of the dried composites was observed using an Environmental Scanning Electron Microscope (ESEM) type Quanta 200, operating at 20 kV with secondary electrons, in low vacuum mode. The cross sections of the samples were performed using a sharp blade to reveal the internal structures. The average diameter of the pores was evaluated from the SEM images using the image analyzing program ACD Photo Editor v3.1.

2.5. Batch Sorption Experiments. Metal ion retention properties of the composites were estimated using a batch equilibrium procedure carried out on a water bath temperature controlled shaker (GFL 1083, Gemini BV). The effect of the initial pH of the solution and of the sorbent dose on the adsorption performance of the beads, at 25 °C, was investigated first, the initial concentration of Cu^{2+} being 444.5 mg/L. The effect of pH on the adsorption capacity of the sorbents was investigated in the pH range 1.5−5.3, at 25 °C, the contact time being 24 h. Thus, about 0.05 g of dried beads were placed in a flask and contacted with 10 mL of the aqueous solution of Cu^{2+}, at different initial pH. The initial pH was adjusted with 2 M HCl or 0.5 M NaOH and was not controlled afterward. The effect of sorbent dose on the amount of the Cu^{2+} bound on the gel was investigated in a similar manner, except the initial solution pH, which was 4.5 (pH of the Cu^{2+} solution), the sorbent dose ranging from 0.025 to 0.2 g.

The amount of the Cu^{2+} ions sorbed at equilibrium, q_e (mg/g), was calculated with eq 2.

$$q_e = \frac{(C_0 - C_e)V}{W_d} \quad (2)$$

where C_o is the initial metal ion concentration (mg/L), C_e is the concentration of metal ions in aqueous solution at equilibrium (mg/L), V is the volume of the aqueous phase (L), and W_d is the amount of the dried sorbent (g). For each adsorption experiment, the average of three independent replicates was reported.

The adsorption removal efficiency of Cu^{2+} ions in aqueous solution was calculated with eq 3

$$R = \frac{C_0 - C_e}{C_0} \times 100 \quad (3)$$

where C_o and C_e have the same meaning as in eq 2.

The experimental adsorption isotherms were generated by varying the initial concentration of Cu^{2+} in the range of 30−4000 mg/L, at pH 4.5, the sorbent dose being 0.05 g/10 mL aqueous solution of Cu^{2+}, at 25 °C. The sorbent was filtered off, and the residual concentration of the metal cation remained in the filtrate was measured by the UV−vis spectroscopy at 808 nm (the maximum absorption wavelengths of $CuSO_4{\cdot}5H_2O$), using a UV−vis SPECORD200 Carl Zeiss Jena, Germany. For the kinetic study, 0.05 g of beads were put in contact with 10 mL of Cu^{2+}, at pH 4.5, the metal concentration being 444.5 mg/L, the concentration of metal ions in the supernatant being measured at different contact durations up to 24 h.

2.6. Error Analysis. Two different error functions were used to determine the validity of the isotherm and of the kinetic models fitted by the nonlinear regression method: coefficient of determination (R^2), and the nonlinear Chi-square (χ^2) test mathematically represented by eq 4

$$\chi^2 = \sum \frac{(q_{e,exp} - q_{e,cal})^2}{q_{e,cal}} \quad (4)$$

If the data from a model are similar to the experimental data, χ^2 is a small number, and if they strongly differ, χ^2 is a big number.

2.7. Desorption and Reuse. Desorption of Cu^{2+} from the beads loaded with the metal ion was performed in 10 mL aqueous solution of 0.1 M HCl, until the Cu^{2+} ions were completely removed from the system (maximum two times). To establish the optimum desorption conditions, the first experiments were conducted as follows: 40 mL of $CuSO_4$ solution with a concentration of 444.5 mg/L and 0.2 g of composite beads were stirred in a water bath temperature controlled shaker (GFL 1083, Gemini BV) at 25 °C, for 24 h. After that, the copper loaded beads were separated from the solution and washed with Milli pore water, subsequently immersed into 40 mL of 0.1 M HCl, and stirred for 1 h. The second step of desorption was similar to the first one, the difference being the volume of eluent which was 20 mL. The volume of the supernatant was measured after each desorption step and the concentration in Cu^{2+} ions was determined by the UV−vis spectroscopy. The regeneration of the composites was performed with 0.1 M NaOH for 1 h while stirring to neutralize H^+ ions, followed by washing several times to neutral pH. The recovered composite beads were employed for another adsorption cycle.

3. RESULTS AND DISCUSSION

3.1. Preparation and Characterization of CS/AOX Composite Beads. Embedding micron-size particles such as organic[51] or inorganic ion exchangers[52] in synthetic polymers or biopolymers, to elaborate composites with enhanced sorption capacity for certain solutes has been reported. Micron-size particles of either AOX or PS-*g*-PAN were embedded in CS matrix in this work. As Scheme 2A shows, in the first step, the reaction mixture consisting of CS, AOX powder thoroughly dispersed in the CS solution, and the corresponding volume of ECH (calculated for a certain molar ratio, according to Table 1) was dropped into TPP 0.05 M aqueous solution to form the composite beads. The influence of the ECH:CS molar ratio on the adsorption properties of heavy metal ions has been investigated by Chen et al.,[5] who found a dramatic decrease in the sorption capacity for an ECH/CS ratio of 3:1. In the present study, ECH was added into the initial reaction mixture (in situ cross-linking), at a molar ratio lower than or equal to 1.7:1 (see Table 1). During the first step of the reaction, the ECH was monofunctionally bound to the CS amine groups, the beads being ionically stabilized. In the second step (2 h in 0.1 M NaOH at 37 °C), the electrostatic interactions between TPP anions and protonated amine groups were partially disrupted, the TPP anions being then released from the beads into the NaOH solution.[41] The covalent cross-linking could occur in basic pH by the interaction between the reformed epoxide ring and the primary amine groups. The post-thermal treatment of the beads in vacuum at 40 °C for 48 h contributed to the increase in the chemical resistance of the beads, increasing the cross-linking by further reactions in solid state between the free NH_2 groups and the nonreacted $-CH_2Cl$.[6,34] As shown in Scheme 2B, the second strategy adopted for preparing CS/AOX composite beads consisted of thorough mixing the PS-*g*-PAN powder in the initial CS solution, the amidoximation of the nitrile groups taking place in situ after the bead formation.

Some optical microscope images are presented in Figure 1 to illustrate the differences between the composite beads as a function of the synthesis conditions. The difference between $CS_{80}AOX_{20}$-A.1 (Figure 1a) and $CS_{75}AOX_{25}$ beads (Figure 1b) consists of the intensity of color, the $CS_{75}AOX_{25}$ beads being almost brown owing to the higher content of AOX, compared to $CS_{80}AOX_{20}$-A.1. The composite beads corresponding to the precursor of $CS_{80}AOX_{20}$-A.2 (CS/(PS-*g*-PAN) (Figure 1c) are white, the PS-*g*-PAN being a white powder. After the in situ amidoximation, the color of the beads in dry state turned light cream.

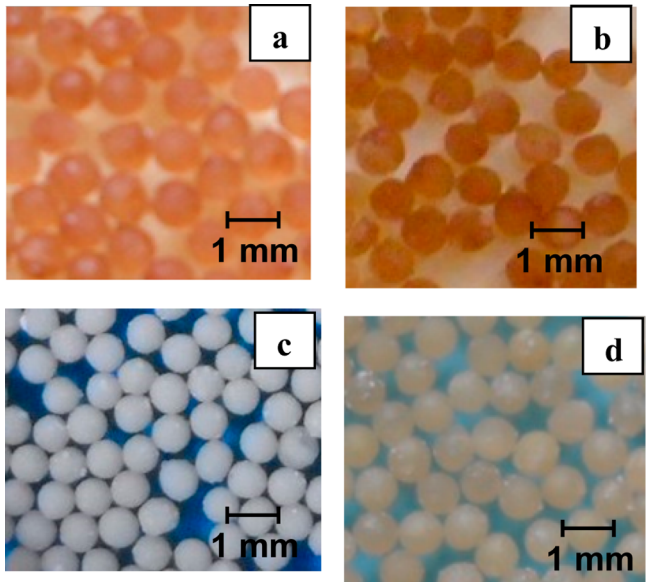

Figure 1. Optical microscope images of composite microspheres in dry state: $CS_{80}AOX_{20}$-A.1 (a), $CS_{75}AOX_{25}$ (b), CS/(PS-*g*-PAN) (c), and $CS_{80}AOX_{20}$-A.2 (d).

To identify the chemical changes of the functional groups, in each stage of the synthesis, FT-IR spectroscopy was used first as a fast tool. The FT-IR spectrum of AOX was compared with the spectrum of the starting copolymer PS-*g*-PAN (not shown here). The following peaks were visible in the spectrum of PS-*g*-PAN: a strong band at 3417 cm^{-1} attributed to the stretching vibration of −OH in PS; a strong band at 2937 cm^{-1} assigned to the asymmetric and symmetric vibration of $-CH_2$ groups; the strong peak located at 2244 cm^{-1} is the characteristic peak of the $-C\equiv N$ groups; the intense peak at 1636 cm^{-1} is due to O−H stretching and bending modes in PS;[14,26] the sharp peak at 1455 cm^{-1} is due to the bending vibration of $-CH_2$ groups; the peaks at 1154 cm^{-1} (antisymmetric stretching of the C−O−C bridge), 1081 and 1025 cm^{-1}, assigned to skeletal vibrations involving C−O stretching, are characteristic of the saccharide structure.[42] The peak located at 2244 cm^{-1} almost disappeared after the amidoximation, and new bands appeared, which support the formation of acrylamidoxime groups, as follows: 1650 cm^{-1}, characteristic of C═N of the oxime group, and 933 cm^{-1} characteristic of the N−O bond in the oxime group.[15,16,18,21] The characteristic peaks of saccharide structure in PS were shifted to 1150, 1103, and 1024 cm^{-1} in the FT-IR spectrum of AOX.

The FT-IR spectra of two composites of CS and AOX prepared by the first strategy (Scheme 2A) are presented in Figure 2A. Figure 2B presents the FT-IR spectra of composite prepared according to the second strategy, both before and after the amidoximation (Scheme 2B).

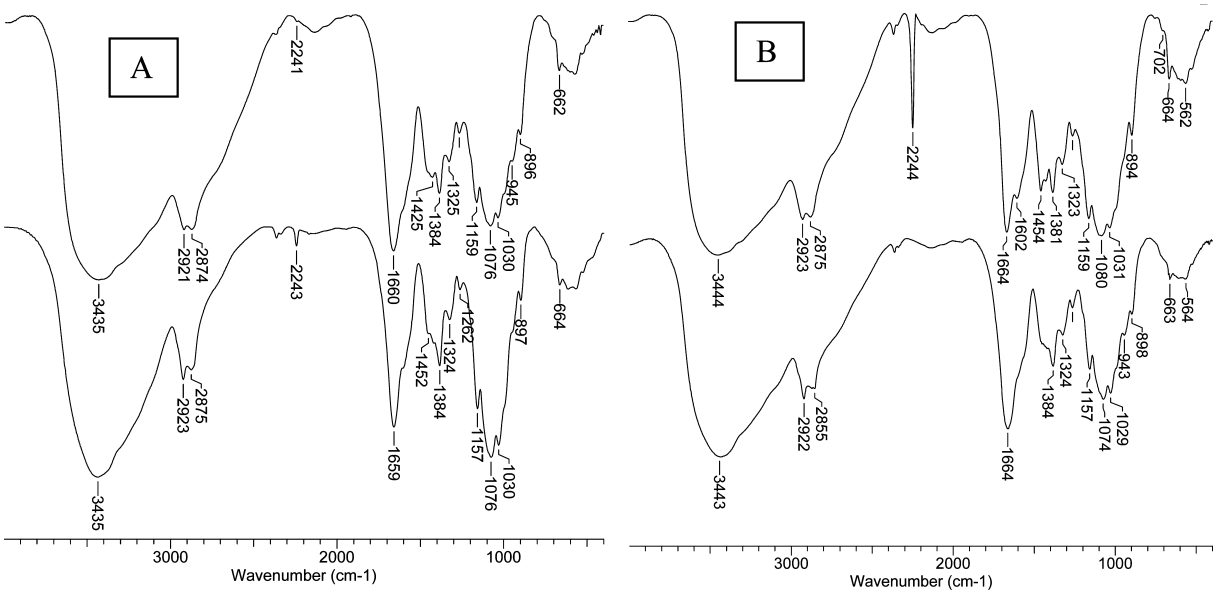

Figure 2. (A) FT-IR spectra of $CS_{80}AOX_{20}$-A.1 (top) and $CS_{80}AOX_{20}$-C (bottom); (B) FT-IR spectra of CS/(PS-*g*-PAN) (top) and $CS_{80}AOX_{20}$-A.2 (bottom).

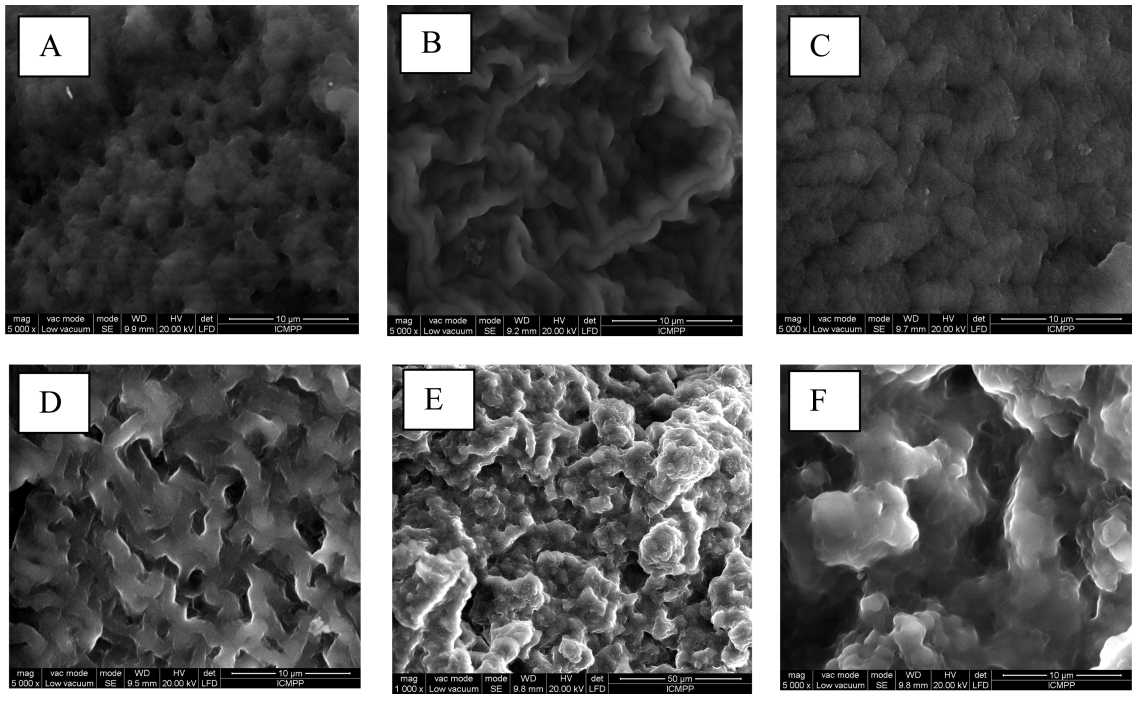

Figure 3. (Top) SEM images of the surface of three composites prepared by embedding AOX in CS matrix (Scheme 2A): (A) $CS_{80}AOX_{20}$-A.1, (B) $CS_{80}AOX_{20}$-C, (C) $CS_{75}AOX_{25}$, the scaling bar and the magnification being 10 μm and 5000×, respectively; (bottom) SEM images of the surface of pristine composite CS/(PS-*g*-PAN) (D) used as precursor in the synthesis of $CS_{80}AOX_{20}$-A2 (E and F), the scaling bar and the magnification being: 10 μm and 5000x (D and F), and 50 μm and 1000× (E).

As Figure 2A shows, in the spectra of $CS_{80}AOX_{20}$-A.1 and $CS_{80}AOX_{20}$-C, the following bands are visible: an overlapped peak at 3435 cm^{-1}, which corresponds to −OH and −NH stretching vibrations; two absorption bands at 2921 and 2874 cm^{-1} attributed to asymmetric and symmetric vibration of $-CH_2$ groups; a strong band at 1660 cm^{-1} and a shoulder at 1600 cm^{-1}, attributed to C═O bond (amide I) and the NH vibration in NH_2 groups (amide II), respectively, in the acetamido groups in the CS matrix; the peaks located at 1425, 1384, and 1325 $cm^{-1}$are attributed to the C−N stretching vibration (amide III);[43] the peaks at 1159, 1076, and 1030 cm^{-1} are assigned to C−O stretching vibration in secondary alcohol, and to the stretching vibration of the C−O−C bridge in anhydroglucose (AGU) units.

Covalent cross-linking reaction in composites CS/AOX with ECH involves mainly primary amino groups in CS.[53] This reaction is supported by the very small peak at around 662 cm^{-1} assigned to the wagging vibration of the free -NH_2 groups, and by the presence of a shoulder around 743 cm^{-1}, assigned to the CH_2 rocking vibration within the $-NH-CH_2-CHOH-$

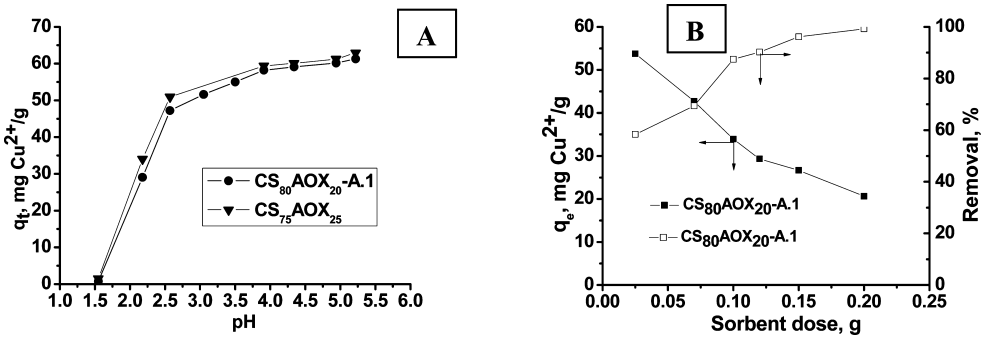

Figure 4. (A) Effect of pH on the sorption capacity of Cu^{2+} by $CS_{80}AOX_{20}$-A.1 and $CS_{75}AOX_{25}$ composites: temperature 25 °C, sorbent dose 0.05 g; (B, left) effect of sorbent dose on the sorption capacity, and (B, right) on the percentage removal of Cu^{2+} at initial pH of 4.9; constant parameters: temperature 25 °C, the initial concentration of Cu^{2+} of 444.5 mg/L, and contact time 24 h.

CH_2-NH- bridge of CS cross-linked with ECH.[43] The small peak located at 896 and 897 cm^{-1}, in $CS_{80}AOX_{20}$-A.1 and $CS_{80}AOX_{20}$-C, respectively, corresponding to P═O stretching and deformation,[42] shows that a small amount of triphosphate anions are still present in the composite microspheres. Figure 2B supports the in situ amidoximation of PS-*g*-PAN entrapped in CS beads. As can be seen, the characteristic band of the $-C\equiv N$ groups located at 2244 cm^{-1} in the spectrum of the CS/(PS-*g*-PAN) composite is absent in the spectrum of $CS_{80}AOX_{20}$-A.2, this being similar to the spectra of the composites obtained by the first strategy (Figure 2A).

As Table 1 shows, the values of *W* at pH 2 were influenced by the synthesis conditions. Thus, for the same ECH/CS molar ratio (1.7:1), the *W* decreased when the beads were kept for a longer time in basic pH during the second step of synthesis ($CS_{80}AOX_{20}$-B), because a higher number of $-NH_2$ groups in CS were involved in the cross-linking reaction. The values of *W* at pH 5.5 were less influenced by the synthesis parameters and synthesis strategy, because CS is low protonated at this pH.

The SEM images of the surface of three CS/AOX composites presented in Figure 3 (top) illustrate the influence of the ECH/CS molar ratio ($CS_{80}AOX_{20}$-A1 compared to $CS_{80}AOX_{20}$-C) and of the CS/AOX weight percentage ($CS_{80}AOX_{20}$-A1 compared to $CS_{75}AOX_{25}$). As can be seen, the decrease of the ECH/CS molar ratio led to a better organization of the composite ($CS_{80}AOX_{20}$-C compared to $CS_{80}AOX_{20}$-A1).

On the other hand, the increase of the AOX content led to a more compact surface of the beads. The SEM images presented in Figure 3 (bottom) show the difference between the surface morphology of the $CS_{80}AOX_{20}$-A.2 composite and the pristine CS/(PS-*g*-PAN) composite beads. Moreover, the SEM image of $CS_{80}AOX_{20}$-A.2 compared to the SEM image of $CS_{80}AOX_{20}$-A.1 support the strong influence of the synthesis strategy on the composite morphology. Thus, while the surface of $CS_{80}AOX_{20}$-A.1, $CS_{80}AOX_{20}$-C, and $CS_{75}AOX_{25}$ is relatively dense, the morphology of $CS_{80}AOX_{20}$-A.2 is characterized by interconnected pores and a less dense morphology. The average diameter of pores evaluated by measuring 12 pores for each image was around 0.92, 1.75, 0.75, and 11.2 μm for $CS_{80}AOX_{20}$-A.1, $CS_{80}AOX_{20}$-C, $CS_{75}AOX_{25}$, and $CS_{80}AOX_{20}$-A.2, respectively. The difference between the morphologies of these composite sorbents could influence their sorption properties for Cu^{2+}, as shown in the next section.

3.2. Sorption of Cu^{2+}. *3.2.1. Influence of Initial pH and Sorbent Dose.* The medium pH of the heavy metal ion solution strongly influences the sorption process because the metal speciation and the surface charge of the sorbent are highly dependent on pH.[29,32,54−56] In this work, the effect of solution pH on the amount of metal ion adsorbed at equilibrium was investigated by varying the initial pH in the range 1.5−5.3, the other parameters being kept constant. As Figure 4A shows, the adsorption capacity of $CS_{80}AOX_{20}$-A.1 and $CS_{75}AOX_{25}$ composites for metal ions increased with increasing solution pH, the values being always higher for the composite beads having a higher content of AOX ($CS_{75}AOX_{25}$). In the discussion of the influence of pH on the sorption of Cu^{2+} onto the CS/AOX composite beads, two characteristics should be considered: the presence of the weak polycation CS, and the amphoteric property of the amidoxime groups.[23,57] In the acidic region, the adsorption is low owing to: (1) the competition between H^+ ions and Cu^{2+} ions for the same active sites (amine groups in CS and AOX) and (2) the electrostatic repulsion between the positive charges of CS and AOX on the one hand and the positively charged metal ions on the other hand.[29,54,55] As Figure 4A shows, the adsorption of Cu^{2+} ions sharply increases with increasing pH from 1.5 to 2.5, monotonously increases up to pH 4.0, and remains almost stable up to 5.2. The Cu^{2+} sorption increased because the protonation degree of amine groups decreased and the surface became less positive, the interactions like ion-exchange and chelating between Cu^{2+} ions and the sorbent surface being thus strengthened. A similar trend has been reported for the sorption of Cu^{2+} on other sorbents.[9,38,54,55] Further increase of pH up to 5.27 led to a slight increase of Cu^{2+} adsorption, for both sorbents. To explain this trend, the pH corresponding to the deposition of $Cu(OH)_2$ was calculated taking into account the K_{SP} (solubility product) of $Cu(OH)_2$ (2.2×10^{-20}) and the initial concentration of Cu^{2+} ions (0.007 mol/L), the result being 5.25. Working at pH values higher than 5.25, when the precipitation of $Cu(OH)_2$ is starting, could lead to inaccurate interpretation of the results and, therefore, for the kinetic and equilibrium measurements, the initial pH of $CuSO_4$ solution was kept constant at 4.5.

As Figure 4B shows, the percentage removal of the metal ion sharply increases up to 100% with the increase of sorbent dose from 0.025 up to 0.2 g. This can be attributed to the increase of the number of sorbent sites available for Cu^{2+} adsorption with the increase of the sorbent dose.

Increasing the sorbent dose, the quantity of metal ion adsorbed per weight unit of sorbent decreased owing to the decrease of the number of metal ions in contact with the sorbent weight unit with the increase of the sorbent dose, this leading to the unsaturation of the adsorption sites during the adsorption process.[54] Since the main objective of the present

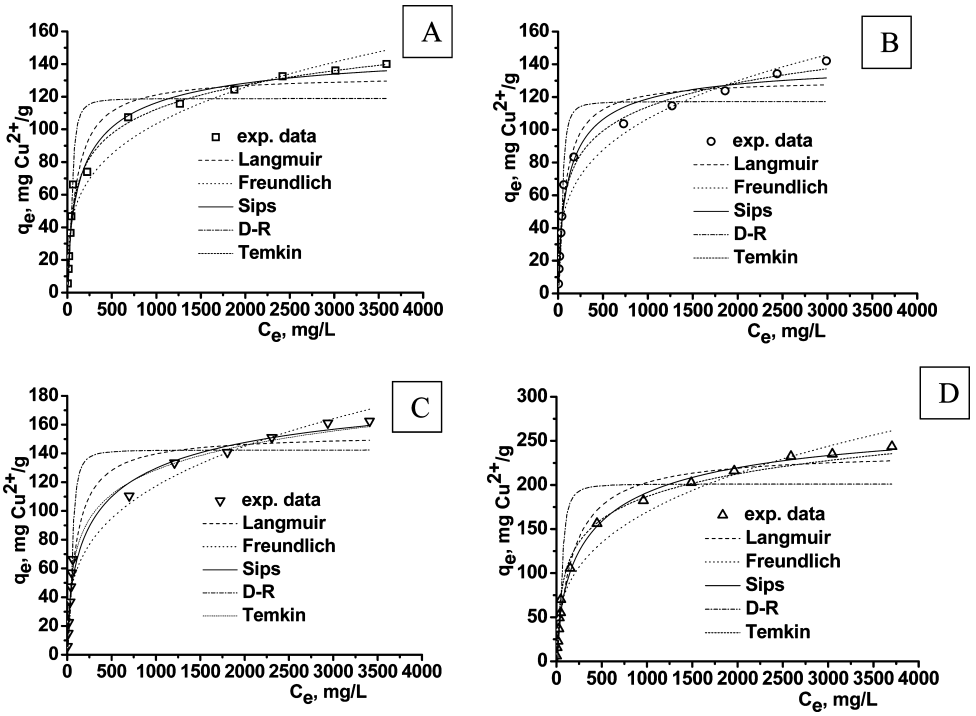

Figure 5. Equilibrium adsorption isotherms of Cu^{2+} onto $CS_{80}AOX_{20}$-A.1 (A), $CS_{80}AOX_{20}$-C (B), $CS_{75}AOX_{25}$ (C), and $CS_{80}AOX_{20}$-A.2 (D) fitted with five isotherm models.

Table 2. Applied Model Isotherms

isotherm	equation	parameters
Langmuir	$q_e = \frac{q_m K_L C_e}{1 + K_L C_e}$	q_m = the theoretical limit of adsorption when the monolayer surface is fully covered with metal ions (mg/g); K_L = the Langmuir constant (L/mg) related to the energy of adsorption
Freundlich	$q_e = K_F C_e^{1/n}$	K_F = Freundlich constant, which predicts the quantity of the metal ion per gram of composite at the equilibrium concentration (mg/g); n = a measure of the nature and strength of the adsorption process and of the distribution of active sites related to the surface heterogeneity; the larger is its value, more heterogeneous is the system
Temkin	$q_e = \frac{RT}{b_T} \ln a_T C_e$	b_T = the Temkin constant related to the heat of sorption (kJ/mol); a_T = the equilibrium binding constant corresponding to the maximum binding energy (L/mg)
D−R	$q_e = q_{DR} \exp\left\{-\beta\left[RT\ln\left(1 + \frac{1}{C_e}\right)\right]^2\right\}$	q_{DR} = the maximum adsorption capacity of the metal ion (mg/g); β = the D−R isotherm constant (mol^2/kJ^2)
Sips	$q_e = \frac{q_m a_S C_e^{1/n}}{1 + a_S C_e^{1/n}}$	q_m = the monolayer adsorption capacity (mg/g); a_S = the Sips constant related to the energy of adsorption; $1/n$ = values close to zero indicate heterogeneous sorbent, while values closer to 1 indicate relatively homogeneous distribution of binding sites; $1/n$ = 1, Sips isotherm coincides with Langmuir equation

study was to show the influence of the chelating sorbent structure on the adsorption properties, the next adsorption experiments were carried out with a sorbent dose of 0.05 mg/10 mL solution of metal ion.

3.2.2. Sorption Isotherms. The experimental isotherms for the sorption of Cu^{2+} ions from aqueous solution onto $CS_{80}AOX_{20}$-A.1, $CS_{80}AOX_{20}$-C, $CS_{75}AOX_{25}$, and $CS_{80}AOX_{20}$-A.2 composite beads are presented in Figure 5. The shape of the isotherms indicates isotherms of type "*L*", where the ratio between the concentration of the metal ion remained in the solution and that adsorbed on the composite beads is a concave curve.[4,55,58]

Fitting the equilibrium data to different isotherm models is performed to establish the most appropriate model to design the sorption of ionic species for large-scale applications.[4,59,60] Therefore, the Cu^{2+} adsorption data were fitted to five isotherm models: two-parameters (Langmuir, Freundlich, Temkin, and Dubinin−Radushkevich (D−R)) isotherm models, and three-parameters (Sips) isotherm model (Table 2) by the nonlinear regression fitting.[4,13,59]

The D−R isotherm constant, β, is related to the mean free energy of adsorption, E (kJ/mol), defined as the free energy when one mole of ion is transferred to the surface of a solid from infinity in solution, and was computed with the following expression:

$$E = 1/(2\beta)^{1/2} \quad (5)$$

The value of E is used to estimate the type of adsorption. The magnitude of E less than 8 kJ/mol indicates that the sorption process is physical in nature, while the values of E between 8 and 16 kJ/mol indicate that the adsorption process proceeds by ion exchange. Chemisorption is characterized by E values higher than 40 kJ/mol.[32,60,61]

Table 3. Isotherm Parameters of Langmuir, Freundlich, Temkin, Dubinin-Radushkevich (D-R), and Sips Models Obtained by Nonlinear Regression Method for the Sorption of Cu^{2+} onto the CS/AOX Composite Sorbents, at 25 °C

isotherm	sorbent	$CS_{80}AOX_{20}$-A.1	$CS_{80}AOX_{20}$-C	$CS_{75}AOX_{25}$	$CS_{80}AOX_{20}$-A.2
Langmuir	q_m (mg/g)	133.15	130.99	153.46	238.14
	K_L (L/mg)	0.01001	0.01205	0.01012	0.00574
	R^2	0.9672	0.9719	0.9715	0.9837
	χ^2	81.48	67.02	100.4	133.62
Freundlich	K_F (mg/g)	14.6	15.03	14.15	17.17
	$1/n$	0.2833	0.2838	0.3061	0.3314
	R^2	0.9453	0.9413	0.9694	0.9704
	χ^2	136.02	139.98	107.65	242.47
Temkin	a_T (L/mg)	0.1849	0.2191	0.1857	0.1519
	b_T (J/mol)	115.17	117.13	100.69	66.61
	R^2	0.9874	0.9847	0.9865	0.9724
	χ^2	31.3	36.49	47.56	225.52
D-R	q_{DR} (mg/g)	118.9	117.24	142.36	201.11
	β (mol^2/kJ^2)	2.9956×10^{-4}	2.69×10^{-4}	3.5907×10^{-4}	4.1208×10^{-4}
	E (kJ/mol)	40.89	43.11	37.32	34.84
	R^2	0.8691	0.8773	0.9171	0.8646
	χ^2	325.73	292.88	292.17	1108.37
Sips	q_m (mg/g)	155.92	143.63	205.16	291.6
	a_S	0.02823	0.02634	0.0318	0.01786
	$1/n$	0.6758	0.7538	0.5776	0.6763
	R^2	0.9777	0.9744	0.9828	0.9953
	χ^2	55.35	61.14	60.35	38.16

The values of the model isotherm parameters, the coefficients of determination (R^2), and nonlinear Chi-square test (χ^2) are presented in Table 3.

Langmuir isotherm assumes monolayer coverage of adsorbate onto a homogeneous adsorbent surface. The fitness of the Langmuir isotherm to the equilibrium sorption data of Cu^{2+} ions onto composites $CS_{80}AOX_{20}$-A.1, $CS_{80}AOX_{20}$-C, and $CS_{80}AOX_{20}$-A.2 is supported by the high values of R^2, which are in the range 0.967−0.984, and the low values of χ^2. The feasibility of adsorption in a certain concentration range can be expressed in terms of a dimensionless constant R_L (eq 6), called constant separation factor or equilibrium parameter[62]

$$R_L = \frac{1}{1 + K_L C_i} \quad (6)$$

where K_L is the Langmuir adsorption constant (L/mg) and C_i is the initial concentration of Cu^{2+} (mg/L).

The adsorption is unfavorable when $R_L > 1$, linear when $R_L = 1$, favorable when $0 < R_L < 1$; irreversible when $R_L = 0$. Herein, the R_L values for the sorption of Cu^{2+} onto the CS/AOX composite sorbents, calculated by eq 6, at different initial concentrations (30−4000 mg Cu^{2+}/L) are as follows: 0.783−0.0244 for $CS_{80}AOX_{20}$-A.1, 0.757−0.0203 for $CS_{80}AOX_{20}$-C, 0.807−0.0241 for $CS_{75}AOX_{25}$, and 0.861−0.0417 for $CS_{80}AOX_{20}$-A.2. As can be seen, the R_L values are ranging between 0.861 and 0.0183 and this indicates that the equilibrium sorption of Cu^{2+} is favorable for all sorbents.

Freundlich isotherm is an empirical equation used to model the adsorption process on heterogeneous surfaces, suggesting that binding sites are not equivalent. The high values of R^2 (>0.94) and the low values of χ^2 also show a high degree of fitness of the Freundlich isotherm to the experimental data, for all the composite sorbents. The values of $1/n < 1$ show the bond energies increase with the surface density and support the feasibility of sorption for all composites. The D−R isotherm was applied to distinguish between physical and chemical sorption. As can be seen (Table 3), the values of q_{DR} are in the same range as q_{max} obtained by fitting the Langmuir isotherm, this reinforcing the applicability of the D−R isotherm in describing the sorption process. The values of mean free energy of adsorption, E, whose magnitude was 40.89 kJ/mol for $CS_{80}AOX_{20}$-A.1and 43.11 kJ/mol for $CS_{80}AOX_{20}$-C would indicate that chemisorption was more probable for these sorbents, while in the case of $CS_{75}AOX_{25}$ and $CS_{80}AOX_{20}$-A.2, where E values were 37.32 and 34.84 kJ/mol, respectively, another type of adsorption would be more important in the adsorption process of Cu^{2+} ions such as ion exchange and chelating mechanisms, simultaneously.[32]

The Temkin isotherm equation assumes that the heat of adsorption of the molecules decreases linearly with coverage due to sorbent−sorbate interactions, and that the adsorption is characterized by a uniform distribution of the bonding energies.[60,67] The Temkin sorption potentials, a_T, are 0.1849, 0.2191, 0.1857, and 0.1519 L/mg for $CS_{80}AOX_{20}$-A.1, $CS_{80}AOX_{20}$-C, $CS_{75}AOX_{25}$, $CS_{80}AOX_{20}$-A.2, respectively, and this would indicate low potential for the CS/AOX composites and Cu^{2+} ions. The Temkin constant, b_T, related to heat of sorption of Cu^{2+} ions were 115.17, 117.13, 100.69, and 66.61 J/mol for $CS_{80}AOX_{20}$-A.1, $CS_{80}AOX_{20}$-C, $CS_{75}AOX_{25}$, and $CS_{80}AOX_{20}$-A.2, respectively. The low values found in this study indicates a weak interaction between sorbate and sorbent. On the basis of the coefficient of determination values (R^2) (>0.98) and the low values of Chi-square (χ^2) for $CS_{80}AOX_{20}$-A.1, $CS_{80}AOX_{20}$-C, and $CS_{75}AOX_{25}$, it can be assumed that the Temkin isotherm is the best isotherm model for these sorbents. This fact would indicate a more heterogeneous surface for these sorbents. A high degree of fitness of the Sips isotherm model on the experimental data, supported by the high value of R^2 (0.9953) and the low value of χ^2 (38.16), was found for the composite $CS_{80}AOX_{20}$-A.2, this fact being attributed to a more homogeneous distribution of the active sites on the surface.

The maximum adsorption capacity, q_m, evaluated by the Langmuir model for the sorption of Cu^{2+} on the composite chelating sorbents synthesized in this work is compared with the values obtained for other sorbents in Table 4.

Table 4. Comparison of Maximum Equilibrium Sorption Capacity of Cu^{2+} on Different Sorbents

sorbent	T (°C)	sorbent dose (g/L)	initial pH	q_m (mg/g)	ref
chitosan-thioglyceraldehyde Schiff's base magnetic resin	30	1	5	76.1	9
starch-*g*-poly(acrylic acid)/sodium humate hydrogel	30	2	4.68	~ 180	11
semi-IPN cryogels	20	0.5	4.7	~ 40	13
poly(amidoxime)/SiO_2 composite	30	4	4.5	100	23
aminated electrospun PAN nanofibers	30	10	4	150.6	29
surface carboxymethylated chitosan hydrogel beads	10−40		5	139	33
chitosan immobilized on bentonite	room temp	~7	4	21.55	35
chitosan cross-linked with epichlorohydrin-triphosphate	25	1	6	130.72	40
porous chitosan-TPP beads	25	1	5	208.3	41
chitosan-tripolyphosphate beads	27	1	4.5	26.06	53
poly(acrylic acid-*co*-acrylamide) hydrogels	25	6	5	121	63
amberlite IRA 402	20	10	6	56.67	64
$CS_{80}AOX_{20}$-A.1	25	5	4.5	133.15	this study
$CS_{75}AOX_{25}$	25	5	4.5	153.46	this study
$CS_{80}AOX_{20}$-A.2	25	5	4.5	238.14	this study

As Table 4 shows, the maximum sorption capacity of Cu^{2+} onto the CS/AOX composite beads is comparable with that of other effective sorbents, and therefore these novel composites could be recommended as an efficient alternative for the sorption of Cu^{2+} ions.

3.2.3. Sorption Kinetics. The effect of contact time on the Cu^{2+} sorption capacity of four CS/AOX composites is presented in Figure 6. The kinetic data were analyzed by three kinetic models, the equations being included in Table 5.

The Lagergren rate equation considers the adsorption rate proportional with the difference between the equilibrium adsorption capacity and the adsorbed amount.[65] The Ho and McKay pseudo-second-order (PSO) kinetic model is based on the assumption that the rate-limiting step is chemisorption, involving valence forces through sharing or exchange electrons between adsorbent and sorbate.[66]

The kinetic data presented in Table 6 indicate that the PSO kinetic model fits the experimental data more accurately than the PFO kinetic model, the R^2 values being higher, and χ^2 being lower for the PSO kinetic model than the corresponding values found for the PFO kinetic model. This suggests that the rate of sorption of Cu^{2+} ions on all composite sorbents depends on the availability of sorption sites and that the rate limiting step may be chemical adsorption.[34,37,54] As can be observed, the values of k_2 increased with the increase in temperature for all sorbents, which indicates a kinetically controlled process.

Sorption of molecules on a sorbent involves several steps, two of them being the most important in an agitated system: the transport of the metal ions through the boundary layer to the sorbent surface, and the transport of solute from the sorbent surface into the pores, called intraparticle diffusion, or inner diffusion, which is usually a slow process.[67,68] However, the PFO and PSO kinetic models do not predict any diffusion mechanism that may control the sorption kinetics. The intraparticle diffusion model proposed by Weber and Morris is commonly used to explain the diffusion mechanism of the adsorption process.[69] C_i term in the Weber and Morris equation (Table 5) gives an idea about the effect of boundary layer thickness, which means the larger the intercept, the greater the contribution of the film diffusion in the rate limiting step. If the plot of q_t versus $t^{0.5}$ gives a straight line, which passes through the origin, then the sorption process is controlled only by intraparticle diffusion.[67,68] If the data exhibit multilinear plots, then two or more steps influence the sorption process.[16,34,67,68] Therefore, to decide on the main rate limiting step, the Webber−Morris equation was applied to the kinetic data obtained for the sorption of Cu^{2+} onto all CS/AOX composite sorbents. As can be seen, the plots of q_t versus $t^{0.5}$ presented in Figure 7 are multilinear: the first region would describe the external resistance to mass transfer, the second region being dominated by the intraparticle diffusion. In the last region, the intraparticle diffusion starts to go slow, owing to the decrease of the Cu^{2+} concentration in the aqueous phase, as well as to the decrease of the active sites available for adsorption. Based on the results presented in Figure 7, we can conclude that the intraparticle diffusion was not the only rate controlling step in the sorption of Cu^{2+} onto the CS/AOX composite beads. The values of k_{id}, C_i, and the correlation coefficients corresponding to the second region of the linear fitting of the kinetic data are listed in Table 7.

As Table 7 shows, the values of k_{id} slightly increased with the increase in temperature for all sorbents, leading to a higher concentration gradient which can cause faster diffusion and sorption.[7] Also, the values of C_i increased with the increase in temperature, for the same sorbent, which reflects the increase of the boundary layer effect. Larger intercepts suggest that surface diffusion has a larger role at high temperatures because of the greater random motion associated with the increased thermal energy. The high values of R^2 indicate that the intraparticle diffusion plays a significant role in the sorption process of Cu^{2+} onto CS/AOX composite beads.

In the case of CS-based sorbents, chelation, electrostatic attraction, and ion exchange may occur at the amino groups, depending on the metal ion and the solution pH, but the hydroxyl groups (especially those located in the C-3 position) may also contribute to the adsorption process.[8] Therefore, to obtain further information about the sorption mechanism of Cu^{2+} onto the CS/AOX beads, the FT-IR spectra of two composites loaded with Cu^{2+} are presented in Figure 8. As Figure 8 shows, the region 3200−3500 cm^{-1} was less affected by the Cu^{2+} uptake. The position and the intensity of the peaks in the region 1700−900 cm^{-1} were significantly changed after the metal ion uptake, as the spectrum of composite $CS_{80}AOX_{20}$-C shows: (1) the peak at 1664 cm^{-1} attributed to the C═O bond (amide I) was shifted to 1655 cm^{-1}; (2) the shoulder at 1600 cm^{-1}, attributed to the absorption intensity of the N−H bending vibration for the primary amine group, was

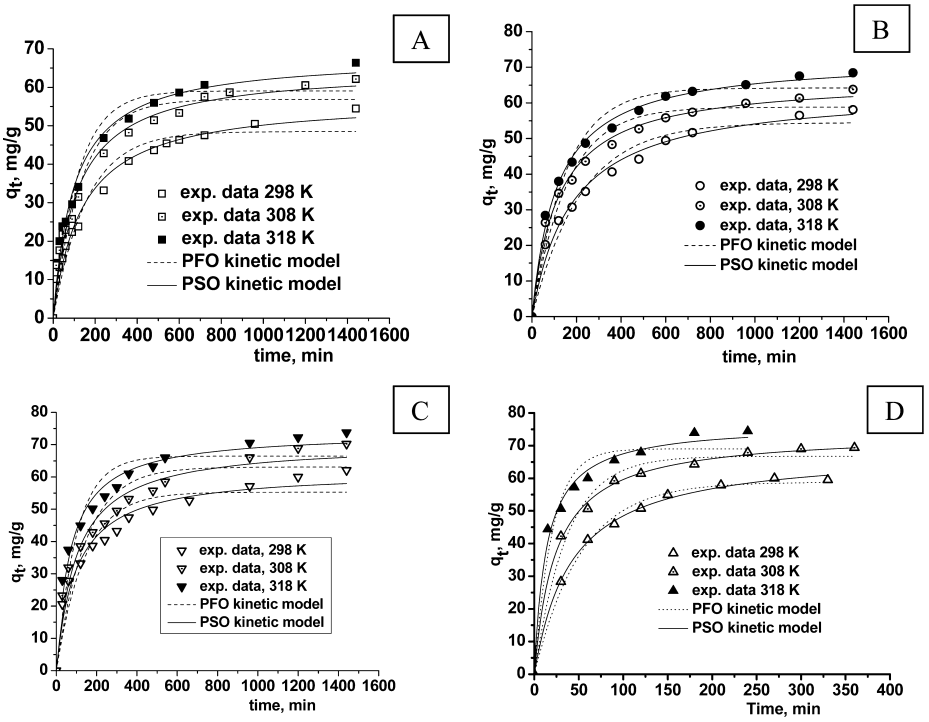

Figure 6. Sorption kinetics of Cu^{2+} onto the CS/AOX composites with different structures: $CS_{80}AOX_{20}$-A.1 (A), $CS_{80}AOX_{20}$-C (B), $CS_{75}AOX_{25}$ (C), and $CS_{80}AOX_{20}$-A.2 (D) at different temperatures; sorbent dose 0.05 g, initial pH 4.5, and initial concentration of Cu^{2+} of 444.5 mg/L.

Table 5. Applied Kinetic Models

kinetic model	equation	parameters
Lagergren rate equation known as seudo-first-order (PFO) kinetic model	$q_t = q_e(1 - e^{-k1t})$	q_e and q_t = the amount of Cu^{2+} ion sorbed at equilibrium (mg/g) and at time t, respectively; k_1 = the rate constant of the PFO kinetic model (min^{-1})
Ho and McKay pseudo-second-order (PSO) kinetic model	$q_t = \frac{k_2 q_e^{\,2} t}{1 + k_2 q_e t}$	q_e and q_t have the same meaning as in the PFO model; k_2 = the rate constant of PSO kinetic model (g mg^{-1} min^{-1}).
Weber and Morris intraparticle diffusion model	$q_t = k_{id} \cdot t^{0.5} + C_i$	k_{id} = the intraparticle diffusion rate constant (g mg^{-1} $min^{-0.5}$); C_i = constant that gives an idea about the effect of boundary layer thickness (mg/g)

Table 6. Kinetic Model Parameters for the Adsorption of Cu^{2+} onto CS_xAOX_y Composite Beads

		PFO kinetic model				PSO kinetic model			
sorbent temp. (K)	$q_{e,exp}$ (mg/g)	$q_{e,calcd}$ (mg/g)	k_1 (min^{-1})	R^2	χ^2	$q_{e,calcd}$ (mg/g)	k_2 (g/mg·min)	R^2	χ^2
				$CS_{80}AOX_{20}$-A.1					
298	54.5	48.5	0.00628	0.9567	12.79	57.08	1.27×10^{-4}	0.9848	4.47
308	62.14	56.86	0.00739	0.9504	19.73	65.0	1.385×10^{-4}	0.9822	7.1
318	66.34	59.07	0.00847	0.9476	22.29	68.14	1.474×10^{-4}	0.9819	7.67
				$CS_{80}AOX_{20}$-C					
298	58.1	54.47	0.00457	0.9568	13.18	63.87	0.868×10^{-4}	0.9872	3.91
308	63.81	61.67	0.00556	0.9371	23.75	71.05	1×10^{-4}	0.9809	7.18
318	68.44	64.2	0.00661	0.9644	14.28	72.73	2.22×10^{-4}	0.9945	2.213
				$CS_{75}AOX_{25}$					
298	60	54.85	0.00724	0.9081	27.4	61.14	1.737×10^{-4}	0.9702	8.88
308	65.5	58.49	0.00901	0.9091	32.06	65.8	1.929×10^{-4}	0.9746	8.95
318	72	65.8	0.0103	0.8114	37.1	73	2.026×10^{-4}	0.9569	8.45
				$CS_{80}AOX_{20}$-A.2					
298	59.5	58.8	0.0191	0.9921	3.057	68.61	3.51×10^{-4}	0.9978	0.84
308	69.4	66.74	0.0273	0.9816	9.95	73.98	5.64×10^{-4}	0.9975	1.21
318	74.43	69.02	0.0494	0.9496	26.46	76.65	9.596×10^{-4}	0.9882	6.19

shifted to 1566 cm^{-1}; (3) the peaks at 1159 and 1076 cm^{-1} attributed to the C−O stretching vibration in secondary alcohol, and to the stretching vibration of the C−O−C bridge in AGU units, diminished and were shifted to 1156 and 1068 cm^{-1}, respectively. All these changes and the presence of additional absorption peaks located at 1108 cm^{-1} and the sharp peak at 617 cm^{-1} in the spectrum of $CS_{80}AOX_{20}$-C, and at 1109 and 616 cm^{-1} in the spectrum of $CS_{80}AOX_{20}$-A.2, support the

dx.doi.org/10.1021/am504480q | ACS Appl. Mater. Interfaces 2014, 6, 16577−16592

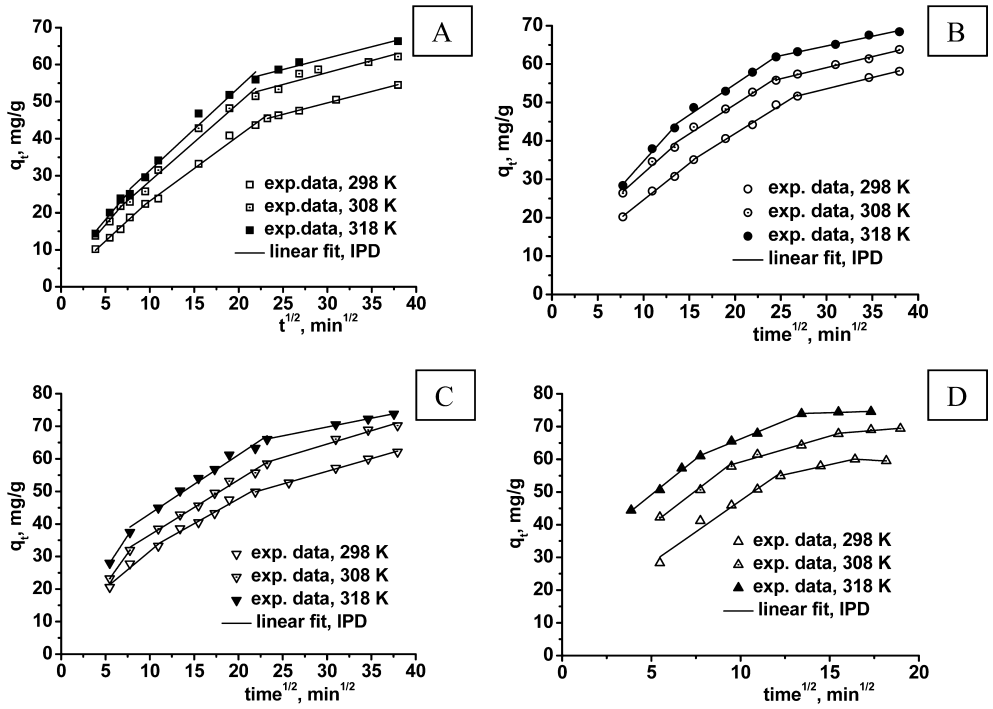

Figure 7. Plots of q_t versus $t^{0.5}$ for the sorption of Cu^{2+} onto the composites $CS_{80}AOX_{20}$-A.1 (A), $CS_{80}AOX_{20}$-C (B), $CS_{75}AOX_{25}$ (C), and $CS_{80}AOX_{20}$-A.2 (D); initial pH 4.5, sorbent dose 0.05 g, and initial concentration of Cu^{2+} of 444.5 mg/L.

Table 7. Kinetic Parameters for the Adsorption of Cu^{2+} onto CS/AOX Composite Beads

	kinetic parameters for intraparticle diffusion		
sorbent/temperature (K)	k_{id} mg/g min$^{0.5}$	C_i mg/g	R^2
	$CS_{80}AOX_{20}$-A.1		
298	1.76	5.58	0.985
308	2.1	7.5	0.977
318	2.23	9.09	0.974
	$CS_{80}AOX_{20}$-C		
298	1.49	12.18	0.991
308	1.53	18.84	0.982
318	1.61	22.65	0.987
	$CS_{75}AOX_{25}$		
298	1.52	17.23	0.972
308	1.69	19.71	0.991
318	1.81	25.02	0.981
	$CS_{80}AOX_{20}$-A.2		
298	1.22	40.4	0.993
308	1.59	43.24	0.972
318	2.23	43.86	0.994

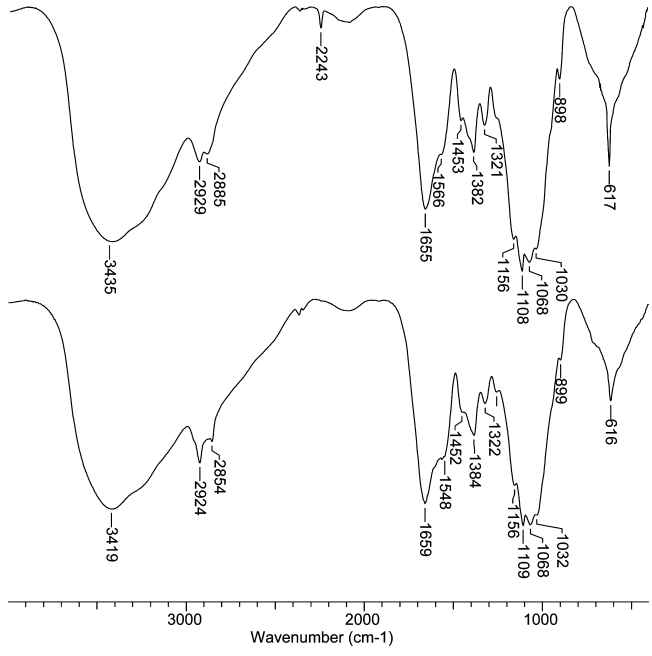

Figure 8. FT-IR spectra of $CS_{80}AOX_{20}$-C (top) and $CS_{80}AOX_{20}$-A.2 (bottom) loaded with Cu^{2+}.

participation of N atoms as the main binding sites in the chelation of Cu^{2+} ions.

The participation of oxygen atoms from OH groups (CS and AOX) is also possible.[23,43]

Figure 9 shows the optical and SEM images of the $CS_{80}AOX_{20}$-A.2 composite loaded with Cu^{2+} ions.

A granular morphology, which retains the characteristics of the irregular granules already seen in Figure 3 (E and F), can be observed (Figure 9, right), but the holes between the granules almost disappeared after the sorption of Cu^{2+}. The whole morphology appears denser than before the sorption of metal ions (the average diameter of pores evaluated by measuring 12 pores being now around 7.3 μm compared to 11.2 μm before adsorption), and supports the strong interaction between the composite sorbent and metal ions. The strong interaction between the amidoxime functional groups in the composite sorbent is also supported by the dark green color of the composite beads (Figure 9, left). The FT-IR spectra and the SEM image support a strong binding of Cu^{2+} ions on the composite sorbents. Owing to the presence of two chelating components in the composite beads, there are various possibilities for binding Cu^{2+} ions on the sorbent, like chelation on two amidoxime groups, chelation on the CS chains by the

Figure 9. Optical (left) and SEM images (mag. 1000×) (right) of the composite $CS_{80}AOX_{20}$-A.2 loaded with Cu^{2+}.

amino and hydroxyl groups, or chelation by the cooperation of the functional groups of both components.

Scheme 3 presents only two possible mechanisms of chelation of Cu^{2+} ions: chelation by the amidoxime groups,

Scheme 3. Two Possible Bindings of Metal Ions onto the CS/AOX Composite Beads

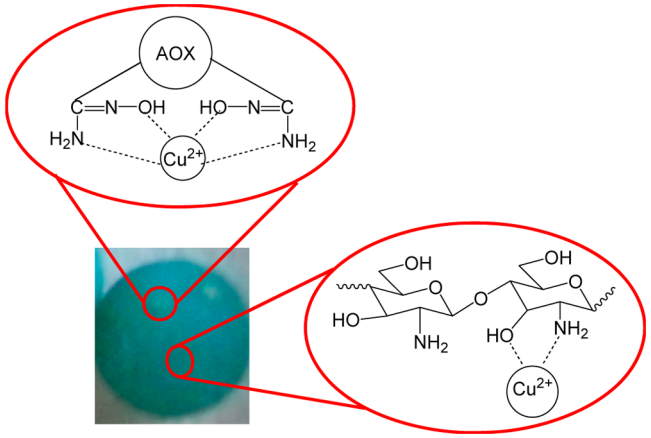

which belong to the entrapped component (AOX), and chelation by the functional groups of the CS matrix.

3.2.4. Thermodynamic Parameters. The thermodynamic parameters, such as free energy of adsorption (ΔG°), enthalpy (ΔH°), and entropy change (ΔS°), can be evaluated by the Van't Hoff equation (eq 7), which correlates ΔH° and ΔS° with either Langmuir constant, K_L,[32,43,58] or equilibrium constant, K_c (eq 8).[16,23,32]

$$\ln K_C = \frac{\Delta S^\circ_{ads}}{R} - \frac{\Delta H^\circ_{ads}}{RT} \quad (7)$$

where R (8.314 J/mol.K) is the gas constant.

$$K_c = \frac{q_e}{C_e} \quad (8)$$

where q_e is the amount of the Cu^{2+} sorbed at equilibrium onto the composite sorbent, mg/g, and C_e is the equilibrium concentration of the metal ion in solution, mg/L, at an initial concentration of 30 mg Cu^{2+}/L (10 mL), equilibrated for 24 h with 0.05 g of composite beads at the optimum pH.

The slope, $\Delta H^\circ/R$ and the intercept $\Delta S^\circ/R$ in Figure 10 obtained by plotting ln K_C versus 1/T according to eq 7 give ΔH° and ΔS° values for the sorption of Cu^{2+} onto the CS/

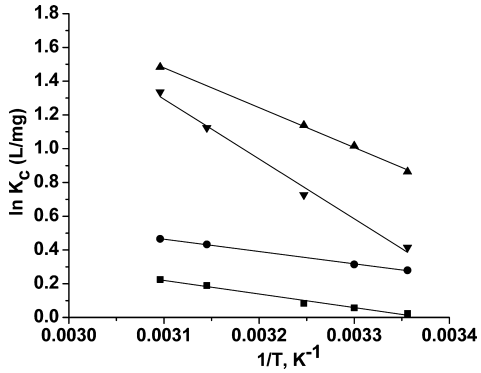

Figure 10. Plot of ln K_c versus $1/T$ for the sorption of Cu^{2+} ions onto: $CS_{80}AOX_{20}$-A.1 (■), $CS_{80}AOX_{20}$-C (●), $CS_{75}AOX_{25}$ (▼), and $CS_{80}AOX_{20}$-A.2 (▲) composite sorbents.

AOX composite sorbents, which are listed in Table 8. On the basis of the values of K_c as a function of temperature, ΔG° values were calculated by eq 9 and listed in Table 8.

$$\Delta G^\circ_{ads} = -RT \ln K_C \quad (9)$$

Table 8. Thermodynamic Parameters of the Cu^{2+} Sorption onto CS/AOX Composite Beads

		thermodynamic parameters		
sample code	temperature (K)	ΔH° (kJ/mol)	ΔS° (J/mol K)	ΔG° (kJ/mol)
$CS_{80}AOX_{20}$-A.1	298	6.69	22.56	−0.0584
	303			−0.144
	308			−0.214
	318			−0.502
	323			−0.603
$CS_{80}AOX_{20}$-C	298	6.07	22.67	−0.691
	303			−0.792
	318			−1.144
	323			−1.25
$CS_{75}AOX_{25}$	298	29.47	102.12	−1.027
	308			−1.86
	318			−2.97
	323			−3.59
$CS_{80}AOX_{20}$-A.2	298	19.64	73.12	−0.257
	303			−2.56
	308			−2.92
	323			−3.586

dx.doi.org/10.1021/am504480q | ACS Appl. Mater. Interfaces 2014, 6, 16577−16592

The negative values of ΔG° for all composite sorbents indicate the sorption is spontaneous and thermodynamically favorable. The increase of the negative value of ΔG° with the increase of temperature suggests an increased trend in the degree of spontaneity of the Cu^{2+} sorption.

The positive values of ΔH° indicate that the adsorption is endothermic and the positive values of ΔS^o show the affinity of sorbents for Cu^{2+} ions and an irregular increase of randomness at the composite-solution interface during the adsorption process.

3.2.5. Desorption and Reusability. As mentioned in section 2.7, the desorption of Cu^{2+} ions with 0.1 M HCl was performed in two steps, two sorbents being considered as examples: $CS_{80}AOX_{20}$-A.1 and $CS_{75}AOX_{25}$. It was found that the percentage removal of Cu^{2+} ions was 99.55 wt %, and 0.45 wt % in the first and the second step of desorption, respectively, for $CS_{80}AOX_{20}$-A.1, and 97.8 wt %, and 2.2 wt % in the first and the second step of desorption, respectively, for $CS_{75}AOX_{25}$. After the regeneration of the composites with 0.1 M NaOH, the recovered composite beads were employed for another adsorption cycle.

The equilibrium sorption capacity of the composites $CS_{80}AOX_{20}$-A.1 and $CS_{80}AOX_{20}$-A.2 for Cu^{2+} ions, as a function of the number of sorption−desorption cycles, is compared in Table 9.

Table 9. Influence of the Sorption/Desorption Cycles on the Equilibrium Sorption Capacity of CS/AOX Composite at 25 °C and Initial Concentration of 444.5 mg Cu^{2+}/L

	adsorption capacity (%)	
number of cycles	$CS_{80}AOX_{20}$-A.1	$CS_{80}AOX_{20}$-A.2
1	100	100
2	98.1	99.7
3	97.8	99.2
4	97.7	98.8
5	96.8	98.5

As Table 9 shows, the equilibrium sorption capacity for Cu^{2+} ions is almost unchanged for both sorbents after five sorption/desorption cycles, the difference consisting of the higher percentage of the sorption capacity preserved in the case of the composite $CS_{80}AOX_{20}$-A.2, i.e. for the composite sorbent prepared by the in situ amidoximation of the nitrile groups, compared to the composite $CS_{80}AOX_{20}$-A.1.

4. CONCLUSIONS

The feasibility of the preparation of novel chelating composites as beads, by ionotropic gelation/covalent cross-linking of a mixture composed of CS, as matrix, and amidoximated PS (AOX), as entrapped component has been demonstrated in the paper. Two strategies were used to synthesis the composite beads: (1) thorough mixing of the AOX powder in the CS solution, followed by bead formation, and (2) thorough mixing of the PS-*g*-PAN as powder in the initial CS solution, followed by bead formation and the amidoximation of the nitrile groups inside the beads. The presence of both components and the covalent cross-linking of the CS/AOX composites was demonstrated by FT-IR spectroscopy, and equilibrium swelling at pH 2. The sorption capacity of the newly synthesized composites for Cu^{2+} ions was evaluated as a function of the ECH:CS molar ratio, the content of AOX in the beads, synthesis strategy, pH, sorbent dose, initial concentration of Cu^{2+} ions, contact duration, and temperature. The synthesis strategy strongly influenced the sorption settlement and the values of the equilibrium sorption capacity, these being faster and, respectively, higher for the composite prepared by the in situ amidoximation of PS-*g*-PAN than for the composite sorbent prepared by the incorporation of the AOX in the CS solution, before the bead formation.

The experimental data were fitted by several isotherm models, out of which Langmuir, Temkin, and Sips isotherm models had high and comparable coefficient of determination (R^2) (0.97−0.99), and hence the best fit. The sorption kinetics, well described by the PSO kinetic model, would indicate the chemisorption as the controlling mechanism of adsorption. On the basis of the sorption kinetic data, on the one side, and the FT-IR spectra and SEM images of the composites loaded with Cu^{2+}, on the other side, a chelation mechanism was suggested. The adsorption process of Cu^{2+} ions onto the CS/AOX composite sorbents was spontaneous ($\Delta G^\circ < 0$) and endothermic ($\Delta H^\circ > 0$). One particular advantage of the composite sorbents presented in the paper is their remarkable chemical and mechanical stability during the successive sorption−desorption cycles, the AOX microparticles also acting as filler for the whole composite.

AUTHOR INFORMATION

Corresponding Author

*Telephone: +40.232217454. Fax: +40.232211299. E-mail: sdragan@icmpp.ro.

Notes

The authors declare no competing financial interest.

ACKNOWLEDGMENTS

This work was supported by CNCSIS-UEFISCSU by the project PN-II-ID-PCE-2011-3-0300.

REFERENCES

(1) Soldatov, V. S.; V. M. Zelenkovskii, V. M.; Orlovskaya, L. A. Sorption of Bivalent Ions by a Fibrous Chelating Ion Exchanger and the Structure of Sorption Complexes. *React. Funct. Polym.* **2011**, *71*, 49−61.

(2) Kim, E.-J.; Lee, C.-S.; Chang, Y.-Y.; Chang, Y.-S. Hierarchically Structured Manganese Oxide-Coated Magnetic Nanocomposites for the Efficient Removal of Heavy Metal Ions from Aqueous Systems. *ACS Appl. Mater. Interfaces* **2013**, *5*, 9628−9634.

(3) Wang, J.; Chen, C. Chitosan-Based Biosorbents: Modification and Application for Biosorption of Heavy Metals and Radionuclides. *Bioresour. Technol.* **2014**, *160*, 129−141.

(4) Gerente, C.; Lee, V. K. C.; Le Cloirec, P.; McKay, G. Application of Chitosan for the Removal of Metals from Wastewaters by Adsorption—Mechanisms and Models Review. *Crit. Rev. Environ. Sci. Technol.* **2007**, *37*, 41−127.

(5) Chen, A.-H.; Liu, S.-C.; Chen, C.-Y.; Chen, C.-Y. Comparative Adsorption of Cu(II), Zn(II), and Pb(II) Ions in Aqueous Solution on the Crosslinked Chitosan with Epichlorohydrin. *J. Hazard. Mater.* **2008**, *154*, 184−191.

(6) Dragan, E. S.; Dinu, M. V.; Timpu, D. Preparation and Characterization of Novel Composites Based on Chitosan and Clinoptilolite with Enhanced Adsorption Properties for Cu^{2+}. *Bioresour. Technol.* **2010**, *101*, 812−817.

(7) Milosavljevic, N. B.; Ristic, M. D.; Peric-Grujic, A. A.; Filipovic, J. M.; Štrbac, S. B.; Zlatko Lj. Rakocevic, Z. L.; Kalagasidis Krušic, M. T. Removal of Cu^{2+} Ions Using Hydrogels of Chitosan, Itaconic Acid and Methacrylic Acid: FTIR, SEM/EDX, AFM, Kinetic, and Equilibrium Study. *Colloids Surf., A* **2011**, *388*, 59−69.

(8) Wan Ngah, W. S.; Teong, L.; Hanafiah, M. A. K. M. Adsorption of Dyes and Heavy Metal Ions by Chitosan Composites: A Review. *Carbohydr. Polym.* **2011**, *83*, 1446−1456.
(9) Monier, M. Adsorption of Hg^{2+}, Cu^{2+}, and Zn^{2+} Ions from Aqueous Solution Using Formaldehyde Cross-Linked Modified Chitosan−Thioglyceraldehyde Schiff's Base. *Int. J. Biol. Macromol.* **2012**, *50*, 773−781.
(10) Kolodynska, D. Adsorption Characteristics of Chitosan Modified by Chelating Agents of a New Generation. *Chem. Eng. J.* **2012**, *179*, 33−43.
(11) Zheng, Y.; Hua, S.; Wang, A. Adsorption Behavior of Cu^{2+} from Aqueous Solutions onto Starch-*g*-Poly(acrylic acid)/Sodium Humate Hydrogels. *Desalination* **2010**, *263*, 170−175.
(12) Sancey, B.; Trunfio, G.; Charles, J.; Minary, J.-F.; Gavoille, S.; Badot, P. M.; Crini, G. Heavy Metal Removal from Industrial Effluents by Sorption on Cross-Linked Starch: Chemical Study and Impact on Water Toxicity. *J. Environ. Manage.* **2011**, *92*, 765−772.
(13) Apopei, D. F.; Dinu, M. V.; Trochimczuk, A.; Dragan, E. S. Sorption Isotherms of Heavy Metal Ions onto Semi-Interpenetrating Polymer Network Cryogels Based on Polyacrylamide and Anionically Modified Potato Starch. *Ind. Eng. Chem. Res.* **2012**, *51*, 10462−10471.
(14) Dash, M.; Chiellini, F.; Ottenbrite, R. M.; Chiellini, E. Chitosan-A Versatile Semi-Synthetic Polymer in Biomedical Applications. *Prog. Polym. Sci.* **2011**, *36*, 981−1014.
(15) Abuilaiwi, F. A.; Atieh, M. A.; Ahmad, M. B.; Ibrahim, N. A.; Ab. Rahman, M. Z.; Wan Yunus, W. M. Z. Preparation and Characterization of Polyamidoxime Chelating Resin from Rubberwood Fibre-*g*-Polyacrylonitrile. *Ads. Sci. Technol.* **2009**, *27*, 661−670.
(16) Shaaban, A. F.; Fadel, D. A.; Mahmoud, A. A.; Elkomy, M. A.; Elbahy, S. M. Synthesis of a New Chelating Resin Bearing Amidoxime Group for Adsorption of Cu(II), Ni(II), and Pb(II) by Batch and Fixed-Bed Column Methods. *J. Environ. Chem. Eng.* **2014**, *2*, 632−641.
(17) Caykara, T.; Alaslan, S. S.; Inam, R. Competitive Adsorption of Uranyl Ions in the Presence of Pb(II) and Cd(II) Ions by Poly(Glycidyl Methacrylate) Microbeads Carrying Amidoxime Groups and Polarographic Determination. *J. Appl. Polym. Sci.* **2007**, *104*, 4168−4172.
(18) El-Hamshary, H.; El-Newehy, M. H.; Al-Deyab, S. S. Oxidation of Phenol by Hydrogen Peroxide Catalyzed by Metal-Containing Poly(Amidoxime) Grafted Starch. *Molecules* **2011**, *16*, 9900−9911.
(19) Kabay, N.; Hayashi, T.; Jyo, A.; Egawa, H. Amidoxime Resins Based on Poly(Acrylonitrile-*co*-vinylidene Chloride-*co*-divinylbenzene) and Their Behavior in Uptake of Uranium from Sea Water. *J. Appl. Polym. Sci.* **1994**, *54*, 333−338.
(20) Huang, F.; Xu, Y.; Liao, S.; Yang, D.; Hsieh, Y.-L.; Wei, Q. Preparation of Amidoxime Polyacrylonitrile Chelating Nanofibers and Their Application for Adsorption of Metal Ions. *Materials* **2013**, *6*, 969−980.
(21) de Santa Maria, L. C.; Amorim, M. C. V.; Aguiar, M. R. M. P.; Guimaraes, P. I. C.; Costa, M. A. S.; Aguiar, A. P.; Rezende, P. R.; de Carvalho, M. S.; Barbosa, F. G.; Andrade, J. M.; Ribeiro, R. C. C. Chemical Modification of Cross-linked Resin Based on Acrylonitrile for Anchoring Metal Ions. *React. Funct. Polym.* **2001**, *49*, 133−143.
(22) Abdel-Razik, H. H.; Kenawy, E.-R. Synthesis, Characterization, and Amidoximation of Diaminomaleodinitrile-Functionalized Polyethylene Thereftalate Grafts for Collecting Heavy Metals from Wastewater. *J. Appl. Polym. Sci.* **2012**, *125*, 1136−1145.
(23) Gao, B.; Gao, Y.; Li, Y. Preparation and Chelation Adsorption Property of Composite Chelating Material Poly(Amidoxime)/SiO_2 Towards Heavy Metal Ions. *Chem. Eng. J.* **2010**, *158*, 542−549.
(24) Horzun, N.; Shahwan, T.; Parlak, O.; Demir, M. M. Synthesis of Amidoximated Polyacrylonitrile Fibers and Its Application for Sorption of Aqueous Uranyl Ions under Continuous Flow. *Chem. Eng. J.* **2012**, *213*, 41−49.
(25) Kang, D. W.; Choi, H. R.; Kweon, D. K. Stability Constants of Amidoximated Chitosan-*g*-Poly(acrylonitrile) Copolymer for Heavy Metal Ions. *J. Appl. Polym. Sci.* **1999**, *73*, 469−476.
(26) Lutfor, M. R.; Silong, S.; Zin, W. M.; Ab Rahman, M. Z.; Ahmad, M.; Haron, J. Preparation and Characterization of Poly-(Amidoxime) Chelating Resin from Polyacrylonitrile Grafted Sago Starch. *Eur. Polym. J.* **2000**, *36*, 2105−2113.
(27) Arnal, N.; Tacconi de Alaniz, M. J.; Marra, C. A. Cytotoxic Effects of Copper Overload on Human-Derived Lung and Liver Cells in Culture. *Biochim. Biophys. Acta, Gen. Subj.* **2012**, *1820*, 931−939.
(28) Arar, Ö.; Yüksel, Ü.; Kabay, N.; Yüksel, M. Removal of Cu^{2+} Ions by a Micro-Flow Electrodeionization (EDI) System. *Desalination* **2011**, *277*, 296−300.
(29) Kampalanonwat, P.; Supaphol, P. Preparation and Adsorption Behavior of Aminated Electrospun Polyacrylonitrile Nanofiber Mats for Heavy Metal Ion Removal. *ACS Appl. Mater. Interfaces* **2010**, *2*, 3619−3627.
(30) Lan, S.; Wu, X.; Li, L.; Li, M.; Guo, F.; Gan, S. Synthesis and Characterization of Hyaluronic Acid-Supported Magnetic Microspheres for Copper Ions Removal. *Colloids Surf., A* **2013**, *425*, 42−50.
(31) Ling, C.; Liu, F.-Q.; Xu, C.; Chen, T.-P.; Li, A.-M. An Integrative Technique Based on Synergistic Coremoval and Sequential Recovery of Copper and Tetracycline with Dual-Functional Chelating Resin: Roles of Amine and Carboxyl Groups. *ACS Appl. Mater. Interfaces* **2013**, *5*, 11808−11817.
(32) Emik, S. Preparation and Characterization of an IPN Type Chelating Resin Containing Amino and Carboxyl Groups for Removal of Cu(II) from Aqueous Solutions. *React. Funct. Polym.* **2014**, *75*, 63−74.
(33) Yan, H.; Dai, J.; Yang, Z.; Cheng, R. Enhanced and Selective Adsorption of Copper(II) Ions on Surface Carboxymethylated Chitosan Hydrogel Beads. *Chem. Eng. J.* **2011**, *174*, 586−694.
(34) Dinu, M. V.; Dragan, E. S. Evaluation of Cu^{2+}, Co^{2+} and Ni^{2+} Ions Removal from Aqueous Solution Using a Novel Chitosan/Clinoptilolite Composite. Kinetics and Isotherms. *Chem. Eng. J.* **2010**, *160*, 157−163.
(35) Futalan, C. M.; Kan, C. C.; Dalida, M. L.; Hsien, K.-J.; Pascua, C.; Wan, M. W. Comparative and Competitive Adsorption of Copper, Lead, and Nickel Using Chitosan Immobilized on Bentonite. *Carbohydr. Polym.* **2011**, *83*, 528−536.
(36) Vandenbossche, M.; Jimenez, M.; Casetta, M.; Bellayer, S.; Beaurain, A.; Bourbigot, S.; Traisnel, M. Chitosan-Grafted Nonwoven Geotextile for Heavy Metals Sorption in Sediments. *React. Funct. Polym.* **2013**, *73*, 53−59.
(37) Deze, E. G.; Papageorgiou, S. K.; Favvas, E. P.; Katsaros, F. K. Porous Alginate Aerogel Beads for Effective and Rapid Heavy Metal Sorption from Aqueous Solutions: Effect of Porosity in Cu^{2+} and Cd^{2+} Ion Sorption. *Chem. Eng. J.* **2012**, *209*, 537−546.
(38) He, J.; Lu, Y.; Luo, G. Ca(II) Imprinted Chitosan Microspheres: An Effective and Green Adsorbent for the Removal of Cu(II), Cd(II), and Pb(II) from Aqueous Solutions. *Chem. Eng. J.* **2014**, *244*, 202−208.
(39) Chiou, M. S.; Li, H. Y. Adsorption Behavior of Reactive Dye in Aqueous Solution on Chemical Cross-Linked Chitosan Beads. *Chemosphere* **2003**, *50*, 1095−1105.
(40) Laus, R.; de Favere, V. T. Competitive Adsorption of Cu(II) and Cd(II) Ions by Chitosan Crosslinked with Epichlorohydrin−Triphosphate. *Bioresour. Technol.* **2011**, *102*, 8769−8776.
(41) Wu, S. J.; Liou, T. H.; Yeh, C. H.; Mi, F. L.; Lin, T. K. Preparation and Characterization of Porous Chitosan−Tripolyphosphate Beads for Copper(II) Ion Adsorption. *J. Appl. Polym. Sci.* **2013**, *127*, 4573−4580.
(42) Mi, F. L.; Shyu, S. S.; Lee, S. T.; Wong, T. B. Kinetic Study of Chitosan-Tripolyphosphate Complex Reaction and Acid-Resistive Properties of the Chitosan-Tripolyphosphate Gel Beads Prepared by in-Liquid Curing Method. *J. Polym. Sci.: Polym. Phys.* **1999**, *37*, 1551−1564.
(43) Kamari, A.; Pulford, I. D.; Hargreaves, J. S. J. Chitosan as a Potential Amendment to Remediate Metal Contaminated Soil—A Characterisation Study. *Colloids Surf. B: Biointerfaces* **2011**, *82*, 71−80.
(44) Espy, H. P. The Mechanism of Wet-Strength Development in Paper: A Review. *Tappi J.* **1995**, *78*, 90−99.

(45) Gamzazade, A. I.; Shimac, V. M.; Skljar, A. M.; Stykova, E. V.; Pavlova, S. A.; Rogozin, S. V. Investigation of the Hydrodynamic Properties of Chitosan Solutions. *Acta Polym.* **1985**, *36*, 420−424.
(46) Brugnerotto, J.; Lizardi, J.; Goycoolea, F. M.; Argüelles-Monal, W.; Desbriéres, J.; Rinaudo, M. An Infrared Investigation in Relation with Chitin and Chitosan Characterization. *Polymer* **2001**, *42*, 3569−3580.
(47) Dragan, S.; Cristea, M.; Arinei, A.; Poinescu, Ig.; Luca, C. Sorption of Aromatic Compounds on Macroporous Anion Exchangers Based on Polyacrylamide: Relation Between Structure and Sorption Behavior. *J. Appl. Polym. Sci.* **1995**, *55*, 421−430.
(48) Dragan, E. S.; Apopei, D. F. Synthesis and Swelling Behavior of pH-Sensitive Semi-Interpenetrating Polymer Network Composite Hydrogels Based on Native and Modified Potatoes Starch as Potential Sorbent for Cationic Dyes. *Chem. Eng. J.* **2011**, *178*, 252−263.
(49) Apopei, D. F.; Dinu, M. V.; Dragan, E. S. Semi-Interpenetrating Polymer Networks Based on Polyacrylamide and Starch or Modified Starch. *Dig. J. Nanomater. Bios.* **2012**, *7*, 707−716.
(50) Li, W.; Liu, R.; Kang, H.; Sun, Y.; Dong, F.; Huang, Y. Synthesis of Amidoxime Functionalized Cellulose Derivatives as a Reducing Agent and Stabilizer for Preparing Gold Nanoparticles. *Polym. Chem.* **2013**, *4*, 2556−2563.
(51) Savina, I. N.; Hanora, A.; Plieva, F. M.; Galaev, I. Y.; Mattiasson, B.; Lozinsky, V. I. Cryostructuration of Polymer Systems. XXIV. Poly(Vinyl Alcohol) Cryogels Filled with Particles of a Strong Anion Exchanger: Properties of the Composite Materials and Potential Applications. *J. Appl. Polym. Sci.* **2005**, *95*, 529−538.
(52) Vincent, C.; Hertz, A.; Vincent, T.; Barre, Y.; Guibal, E. Immobilization of Inorganic Ion-Exchanger into Biopolymer Foams—Application to Cesium Sorption. *Chem. Eng. J.* **2014**, *236*, 202−211.
(53) Bocourt, M.; Arguelles-Monal, W.; Cauich-Rodríguez, J. V.; May, A.; Bada, N.; Peniche, C. Interpenetrated Chitosan-Poly(Acrylic Acid-Co-Acrylamide) Hydrogels. Synthesis, Characterization and Sustained Protein Release Studies. *Mater. Sci. Appl.* **2011**, *2*, 509−520.
(54) Wan Ngah, W. S.; Fatinathan, S. Adsorption Characterization of Pb(II) and Cu(II) Ions onto Chitosan-Tripolyphosphate Beads: Kinetic, Equilibrium and Thermodynamic Studies. *J. Environ. Manage.* **2010**, *91*, 958−969.
(55) Anirudhan, T. S.; Divya, L.; Bringle, C. D.; Suchithra, P. S. Removal of Copper(II) and Zinc(II) from Aqueous Solutions Using a Lignocellulosic-Based Polymeric Adsorbent Containing Amidoxime Chelating Functional Groups. *Sep. Sci. Technol.* **2010**, *45*, 2383−2393.
(56) Guibal, E. Interactions of Metal Ions with Chitosan-Based Sorbents: A Review. *Sep. Purif. Technol.* **2004**, *38*, 43−74.
(57) Eloy, F.; Lenaers, R. The Chemistry of Amidoximes and Related Compounds. *Chem. Rev.* **1962**, *62*, 155−183.
(58) Giles, C. H.; Smith, D.; Huitson, A. A General Treatment and Classification of the Solute Adsorption Isotherm. I. Theoretical. *J. Colloid Interface Sci.* **1974**, *47*, 755−765.
(59) Foo, K. Y.; Hameed, B. H. Insights into the Modeling of Adsorption Isotherm Systems. *Chem. Eng. J.* **2010**, *156*, 2−10.
(60) Vasiliu, S.; Bunia, I.; Racovita, S.; Neagu, V. Adsorption of Cefotaxime Sodium Salt on Polymer Coated Ion Exchange Resin Microparticles: Kinetics, Equilibrium and Thermodynamic Studies. *Carbohydr. Polym.* **2011**, *85*, 376−387.
(61) Chen, H.; Wang, A. Adsorption Characteristics of Cu(II) from Aqueous Solution onto Poly(Acrylamide)/Attapulgite Composite. *J. Hazard. Mater.* **2009**, *165*, 223−231.
(62) Hall, K.; Eagleton, L. C.; Acrivos, A.; Vermeulen, T. Pore- and Solid-Diffusion Kinetics in Fixed-Bed Adsorption under Constant-Pattern Conditions. *Ind. Eng. Chem. Fundam.* **1966**, *5*, 212−223.
(63) Orozco-Guareño, E.; Santiago-Gutiérrez, F.; Morán-Quiroz, J. L.; Hernandez-Olmos, S. L.; Soto, V.; de la Cruz, W.; Manríquez, R.; Gomez-Salazar, S. Removal of Cu(II) Ions from Aqueous Streams Using Poly(Acrylic Acid-*co*-acrylamide) Hydrogels. *J. Colloid Interface Sci.* **2010**, *349*, 583−593.
(64) Kolodynska, D. Cu(II), Zn(II), Co(II) and Pb(II) Removal in the Presence of the Complexing Agent of a New Generation. *Desalination* **2011**, *267*, 175−183.
(65) Lagergren, S. *Kungliga Svenska Vetenskapsakademiens Handlingar* **1898**, *24*, 1−39.
(66) Ho, Y. S.; McKay, G. The Kinetics of Sorption of Basic Dyes from Aqueous Solution by Sphagnum Moss Peat. *Can. J. Chem. Eng.* **1998**, *76*, 822−827.
(67) Srivastava, Y. C.; Swamy, M. M.; Mall, I. D.; Prasad, B.; Mishra, I. M. Adsorptive Removal of Phenol by Bagasse Fly Ash and Activated Carbon: Equilibrium, Kinetics and Thermodynamics. *Colloids Surf., A* **2006**, *272*, 89−104.
(68) Ma, J.; Yu, F.; Zhou, L.; Jin, L.; Yang, M.; Luan, J.; Tang, Y.; Fan, H.; Yuan, Z.; Chen, J. Enhanced Adsorptive Removal of Methyl Orange and Methylene Blue from Aqueous Solution by Alkali-Activated Multiwalled Carbon Nanotubes. *ACS Appl. Mater. Interfaces* **2012**, *4*, 5749−5760.
(69) Weber, J. W. J.; Morris, J. C. Kinetics of Adsorption on Carbon from Solution. *J. Sanit. Eng. Div., Am. Soc. Civ. Eng.* **1963**, *89*, 31−60.